Challenge Journal of
CONCRETE RESEARCH LETTERS

Vol.11 No.4 (2020)

acoustic emission artificial neural network
compressive strength concrete
corrosion cracking curing ductility
durability energy absorption ferrocement
flaky aggregate fly ash fracture mortar
palm oil fuel ash reinforced concrete
scrap self-compacting concrete silica fume
strengthening superplasticizer tensile strength
waste disposal water absorption w ility

ISSN 2548-0928

TULPAR
ACADEMIC PUBLISHING

Challenge Journal of Concrete Research Letters

E-mail: *cjcrl@challengejournal.com*

Web page: *cjcrl.challengejournal.com*

TULPAR Academic Publishing
www.tulparpublishing.com

Challenge Journal of Concrete Research Letters

CONTENTS

Research Articles

TULPAR ACADEMIC PUBLISHING

Challenge Journal of Concrete Research Letters

Research Article

The physico-mechanical properties of concrete with red-mud at high temperatures

Ibrahim A. Alameri [a,b,*], Meral Oltulu [b]

[a] *Department of Civil Engineering, Sana'a University, Sana'a 13341, Yemen*
[b] *Department of Civil Engineering, Atatürk University, Erzurum 25240, Turkey*

ABSTRACT

Reuse of treated waste can provide significant environmental, social and economic benefits. It is necessary to use it in the right places while keeping the properties of the waste in mind. Aluminum-rich wastes such as red mud derived from bauxite may be used in places exposed to high temperatures. This article discusses the effects of high temperatures of 25, 200, 300, 400, 600 and 800°C and 3 hours of exposure on concrete samples replaced by red mud at 0, 10, 15 and 20%. To study the concrete's mechanical and permeability properties, loss in weight, compressive strength, splitting tensile strength, capillary water absorption and water permeability tests were performed for all mixes. Results were closer to those of the control specimen, which ultimately supported the use of red mud at a ratio of 10%.

ARTICLE INFO

Article history:
Received 18 June 2020
Revised 20 July 2020
Accepted 11 August 2020

Keywords:
Waste materials
Red-mud
Elevated temperatures
Mechanical properties
Permeability
Capillary water absorption

1. Introduction

The physicochemical, mechanical properties and microstructure of concrete during or after exposure to high temperatures are required to predict its structural behavior and capacity. Concrete may be exposed to high temperatures in areas such as nuclear reactors, near furnaces, areas exposed to fire and areas exposed to jet engine explosions. Additionally, most buildings and infrastructure face a major fire risk. In order to understand the behavior of concrete at high temperatures or under fire, the most appropriate parameters were identified and investigated. These parameters related to the type of concrete that is used include exposure time, temperature increase rate, concrete age, type of aggregate used, type of cement used, type of different additives, and water/cement ratio.

Concrete seems to be exposed to no significant damage when subjected to temperatures up to 200°C, but for higher temperatures than 200°C, it is essential to study the exposure conditions and the employed concrete. The effect of high temperatures on normal concrete is summarized in Table 1.

Waste materials exhibiting other pozzolanic properties that are used in concrete include silica fume, fly ash, blast furnace slag, calcined clay and alkali-activated slag cement (Ardahanlı et al., 2019; Alameri et al., 2019; Alameri and Oltulu, 2019). In addition to these materials, red mud derived from bauxite is also among the recently researched materials. Moreover, alumina is known to have a high resistance to high temperature, and red mud contains a high content of alumina. Today, approximately 120 million tons of red mud is produced annually, and it is not satisfactorily disposed of or recycled. Traditionally, the method of red mud disposal in ponds often has adverse environmental effects during the monsoon period.

The waste causes pollution of groundwater when the red mud gets mixed with water, and underground water resources such as wells or aquifer may get polluted by alkali seepage, impact on plant life, alkaline air born dust is carried with air and has effects on the transpiration process of plants, resulting in reduction of plant life. This may also include soil properties changed by land disposal, which results in reduced fertility when this waste is mixed with fertile land, vast areas of land are consumed

* *Corresponding author*. E-mail address: i.ameri@eng-su.edu.ye (I. A. Alameri)
ISSN: 2548-0928 / DOI: https://doi.org/10.20528/cjcrl.2020.04.001

because of dumping of red mud, and if service reservoirs get polluted, it may create hurdles for the society (Sawant et al., 2012; Rathod et al., 2014; Rana and Sathe, 2015).

In order to reduce these harmful effects, studies were carried out on red mud in road construction, cementitious products, stabilization material and wastewater treatment areas (Hu et al., 2018). Moreover, a limited number of studies have been conducted on the topic of concrete. In these studies, red mud was used instead of cement partially to investigate the cementitious properties of the composites. A lot of studies have been performed on the ratio of the red mud that is used, and these are presented in Table 2.

Table 1. Effects of temperature on concrete (Baradan et al., 2010).

Temperature	Effect
100–150°C	Evaporation of free moisture in the concrete mass takes place.
150–250°C	Shrinkage, crack formation, degradation in tensile strength, pinkish color.
250–300°C	Aluminum and iron oxide compounds, loss of body water, decrease in compressive strength.
400°C	$Ca(OH)_2$ converted into CaO (33% degradation in volume).
400–600°C	Destruction in the structure of CSH, gray-white color, degradation in compressive strength would be 80%.

Table 2. Red mud studies, experiments and optimum red mud ratio.

	Authors	Red mud ratio	Experiments	Optimum ratio of red mud
1	Ribeirol et al. (2010)	10, 20, and 30%	Compressive strength	10%
2	Rathod et al. (2014)	5, 10, 15, 20, 25, 30, and 40%	Compressive, and split tensile strength test	25%
3	Bishetti and Pammar (2014)	0, 5, 10, 15, 20, and 25%	Compressive, and split tensile strength	20%
4	Manfroi et al. (2014)	5, 10, and 15%	Pozzolanic activity, compressive strength, and water absorption by capillarity	5%
5	Rana and Sathe (2015)	10%, 15, 20, and 25% with addition of 4, 8 and 12% lime to the weight of red mud	Compressive strength	10% with 4% lime
6	Rathod et al. (2015)	10, 15, and 20% with 5% lime	Compressive, split tensile, and flexural strength	10%
7	Metilda et al. (2015)	5, 10, 15, 20, and 25%	Compressive, split tensile, and flexural strength	15%
8	Liu and Poon (2016)	Fly ash was replaced by red mud at 0, 25, 50, 75 and 100% by weight	Fresh self compacting concrete tests, compressive, split tensile strength, and drying shrinkage	50%
9	Tang (2014)	0-30%	Fresh self compacting concrete tests, compressive, splitting tensile strength, and microstructural test	20%
10	Oltulu and Alameri (2019)	10% red mud with 0.5, 1 and 1.25% of nano-alumina ratios	Compressive, and splitting tensile strength	%10 with 0.5% nano-alumina

As seen in Table 2, the literature does not offer exact information about the optimum proportion of red mud, and a detailed study on red mud which is very rich in alumina at high temperatures is missing in the literature. Due to this limitation in the literature, this experimental study is needed for a better understanding of the effects of temperature on addition of red mud (RM) into concrete. The goals of this study for these reasons were:

a) To find a solution for the aforementioned environmental problems and look for economically viable recycling of red mud alternatives as a component of building materials, this study was conducted to investigate the optimum ratio of red mud as a partial replacement for cement.
b) The feasibility of utilizing the Bayer red mud and investigation of the optimum red mud ratio in concrete at high temperatures are demonstrated. This study will draw attention to increasing the use of aluminum containing waste materials, which will have a positive effect especially at high temperatures in concrete.
c) There has been limited research on red mud in concrete, and in particular, there were no studies on physico-mechanical properties after high temperature treatment. It is expected that this article will illuminate the literature since which the physico-mechanical properties of waste red mud with high alumina content will be determined after applying high temperature.

For the aforementioned reasons, an experimental study was performed by replacing cement with red mud by 0-20% to investigate the optimum percentage of red mud that can be used in concrete and study the effects of materials that have a high content of alumina such as red mud against high temperatures.

2. Material and methods

2.1. Material

Ordinary Portland cement (CEM II 42.5 R) conforming to TS EN 197-1 (2012) and TS EN 196-1 (2016), which is compatible with the European standard, and red mud with index and chemical properties shown in Table 3 were used to produce C40/50 Concrete. Standard 100-mm-diameter and 200-mm-high test cylinders and 150x150x150 test cubes were cast. RM thermal decomposition is shown in the TGA–DTA diagram. With rising temperatures, three weight loss steps were observed in the profile as explained in Table 4 and shown in Fig. 1 (Nath et al., 2015). Fine and coarse aggregate properties listed in Table 5 were used, and tests of specific gravity and water absorption were conducted according to the Turkish standard TS EN 1097-6, 2013, which is compatible with the European standard. Superplasticizer with a density of 1.045 gr/cm^3 and gray/green color based on modified polycarboxylate were added to water before mixing the concrete by 0.75% of the cementitious material.

Table 3. Index and chemical properties of RM and PC.

	RM	PC
Chemical composition (%)		
SiO_2	18,95	17,6
Al_2O_3	25,65	4,45
Fe_2O_3	36,94	3,08
CaO	3,30	60,02
MgO	-	2,29
SO_3	-	2,67
Loss on ignition	17,75	8,49
Na_2O	7,04	0,22
K_2O	-	0,63
Na2O+0,658K2O	-	0,63
Cl	-	0,0144
Unmeasured	-	0,54
Free CaO	-	0,69
Total additives	-	19,9
TiO_2	5,62	-
Others	2,51	-
index properties		
Specific gravity	3.05	3,01
Specific surface (cm²/g)	-	4403
Compressive strength (MPa)	-	51,03
pH	12-13	-

Table 4. Effect of temperature in red-mud.

Temperature	Effect
25–260°C	Weight loss about 4.3% of total weight the reason is that the evaporation of water.
260–325°C	Weight loss about 8.9% of the total weight the reason is that the loss of H_2O from the sample as a whole and also the removal of H_2O from $Al(OH)_3$.
325–500°C	Weight loss about 10.9% of the total weight due to the release of CO_2 during the decomposition of $CaCO_3$.

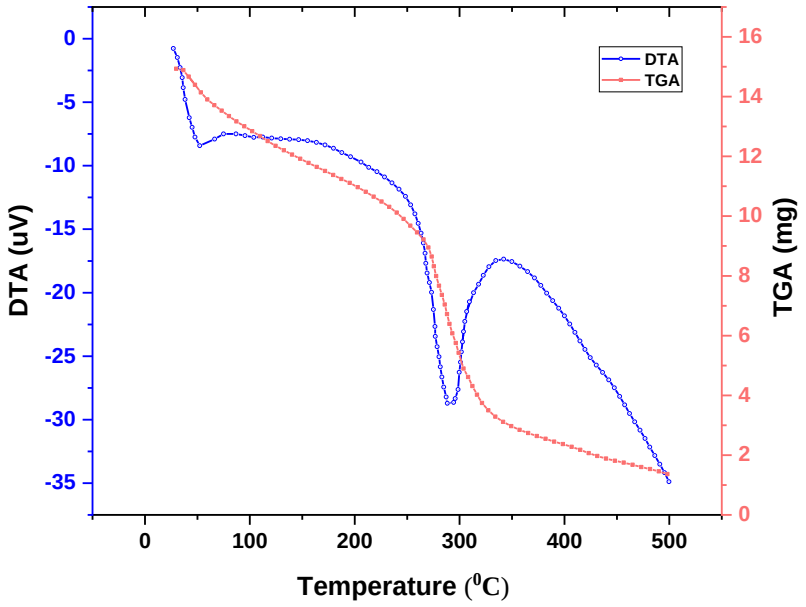

Fig. 1. TGA–DTA diagram of RM in the temperature range of 28°C to 500°C (Nath et al., 2015).

Table 5. Properties of aggregate.

Aggregate size (mm)	Specific Gravity	Water Absorption (%)	Stock Humidity (%)
0-2	2.686	1.77	1.8
2-4	2.671	1.75	1.1
4-8	2.652	1.92	1.0
8-16	2.664	1.56	0.8
16-25	2.678	1.36	0.7

2.2. Concrete mix proportion

Concrete mix design was carried out by using TS EN 206 (2014). C40/50 concrete with a water/binder ratio of 0.48 was produced as a control mix. Four different mix proportions were selected. Red mud replaced 10, 15, and 20% of cement by weight. The mix proportions are listed in Table 6.

Table 6. Concrete mix proportions.

Materials used	C	RM	Aggregate					W	SP's	W/C+RM
			0-2 (mm)	2-4 (mm)	4-8 (mm)	8-16 (mm)	16-25 (mm)			
Units	kg/m³	kg/m³	kg/m³	kg/m³	kg/m³	kg/m³	kg/m³	kg/m³	kg/m³	-
0RM	416.4	-	641.00	206.45	240.27	498.38	137.69	199.64	3.123	0.48
10RM	374.76	41.64	641.00	206.45	240.27	498.38	137.69	199.64	3.123	0.48
15RM	353.94	62.46	641.00	206.45	240.27	498.38	137.69	199.64	3.123	0.48
20RM	333.12	83.28	641.00	206.45	240.27	498.38	137.69	199.64	3.123	0.48

2.3. Experiments

Reduction of the amount of cement by replacing concrete with red mud was explored by comparing the mechanical properties of the samples. Moreover, the physico-mechanical properties of concrete with red mud were evaluated after exposure to high temperature.

2.3.1. High temperature test

The concrete samples were removed from water and dried in air for 1 day at 60% and 25°C mean relative humidity and temperature, respectively (Fig. 2). The samples were then placed in an electrical oven at 100°C for 24 hours before exposing them to high temperatures, while this step was found to be necessary to prevent the concrete samples from exploding in the oven due to the steam formation (Tanyıldızı and Erol, 2018; Ruano et al., 2018; Toric et al., 2014). After that, an electrical oven designed for a maximum temperature of 1200°C was used to heat the concrete samples to 200, 300, 400, 600 and 800°C, with a total duration in the furnace of 3 hours for each temperature (Beglarigale et al., 2016, Sanchayan and Foster, 2016).

2.3.2. Loss in weight

This test was made to measure the moisture mass conservation within the system. During the heating process, moisture is transposed from the specimen to the environment. The specimens were weighed before heating (wi) and after cooling (ws) with an accuracy of 1gm. The changes in specimen weight (W) are expressed as percentages of the initial weights by using the following Eq. (1):

$$W\ (\%) = \frac{w_i - w_s}{w_i} \times 100 \quad (1)$$

2.3.3. Compressive and splitting tensile strength tests

Compressive and Splitting tensile strength tests were conducted based on the TS EN 12390-3, 2019 and TS EN 12390-6, 2010 standards.

2.3.4. Water permeability test

Water permeability test was carried out according to the German Standard DIN 1048 (1991). 200x100 mm cylindrical concrete specimens were exposed to a water pressure of 500 kPa for a period of 72 hours. At once after the end of the tests, the specimens were cut and measured for the depth of water penetration.

2.3.5. Capillary water absorption test

Capillary water absorption test was conducted in accordance with the standard ASTM C1585 (2013). Cube specimens of 150x150x150 mm were used. The sides of the specimens were sealed with tape up to 40 mm in height so that only one face of the specimen was subjected to water. The weight of the specimens was observed over a period of time (0– 24 h) during contact with water.

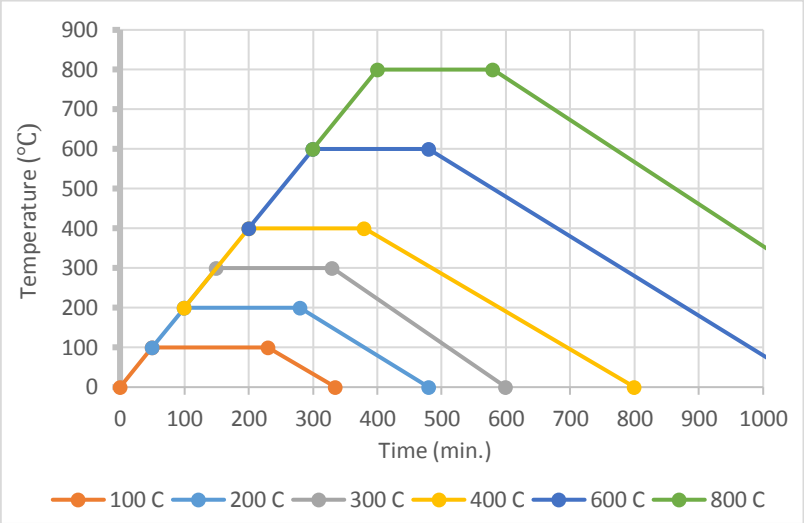

Fig. 2. Heating profile (Alameri, 2017).

3. Results and Discussions

3.1. Loss in weight

The weight of the specimens was measured before and after subjecting them to different temperatures. The weight loss increased with the increase in the maximum exposure temperatures due to accelerated drying. These results agreed with those in the literature (Sancak et al., 2008; Alsheikh 2011). The amount of loss in weight as a percentage is shown in Table 7 and Fig. 3. The Samples with and without RM were subjected to high temperatures, and the highest weight losses for 200°C, 300°C and 400°C were observed in 15RM, whereas those for 600°C and 800°C were observed in 20RM. The increased weight loss was because of the dehydration of the hydration products and the loss of water from the fine pores in the cement paste and aggregate particles. The relationship between the weight loss and the temperature of exposure was non-linear. The 15RM and 20RM concretes showed higher weight losses in comparison to the control concrete, which may be due to the high percentage of red mud. According to the study reported by Nath et al. (2015), three weight loss steps occurred as the temperature increased (Fig. 1).

Table 7. Loss in weight of concrete (%).

Temperature	0RM	10RM	15RM	20RM
25°C	0	0	0	0
200°C	0.76	0.8	0.98	0.67
300°C	1.65	1.40	3.50	3.40
400°C	6.26	6.10	6.90	6.70
600°C	8.29	8.80	8.90	9.10
800°C	11.04	11.20	12.20	12.50

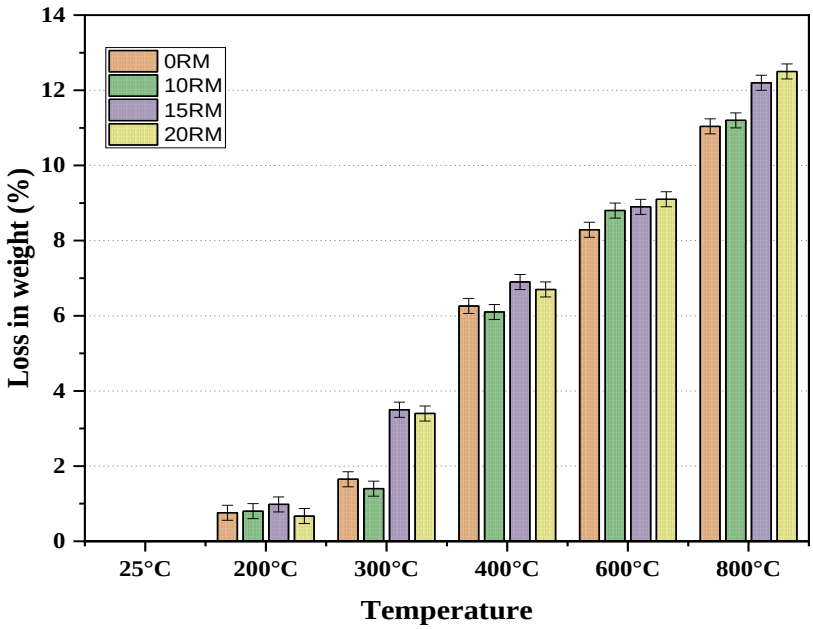

Fig. 3. Loss in weight of concrete at different temperatures.

3.2. Compressive and splitting tensile strengths

3.2.1. Compressive strength

At 25°C, the control mixture 0RM achieved a compressive strength of 41.5 MPa. The mixtures 10RM, 15RM and 20RM achieved compressive strengths of 39.8 MPa, 35.4 MPa and 30.6 MPa, respectively. The compressive strength reached an optimum value at 10RM and then decreased for 15RM and 20RM. A decrease in strength of 4.3%, 14.8% and 26.3% was observed for 10RM, 15RM and 20RM, respectively in comparison to 0RM. The results are shown in Table 8 and Fig. 4.

3.2.2. Splitting tensile strength

Table 9 and Fig. 5 show that, at 25°C, the control mixture 0RM achieved a splitting tensile strength of 4.2 MPa. The mixtures 10RM, 15RM and 20RM achieved splitting tensile strengths of 4.1 MPa, 4.2 MPa and 3.0 MPa, respectively. The splitting tensile strength reached an optimum value at 15RM and 10RM, and the maximum loss in strength was in 20RM. These results showed that the addition of RM reduces the compressive and the splitting tensile strength of concrete. Moreover, these results were compatible with the literature (Rathod et al., 2014; Tang, 2014; Kushwaha et al., 2013; Bishetti and Pammar, 2014).

Table 8. Compressive strength of concrete at different temperatures.

	Compressive strength (MPa) (to their initial 25°C strengths %)				Variation vs. control specimen (%)		
Temperature	0RM	10RM	15RM	20RM	10RM	15RM	20RM
25°C	41.5	39.8	35.4	30.6	-4.3	-14.8	-26.3
200°C	30.4(-26.7%)	34.5(-13.3%)	26.4(-25.4%)	30.3(-1.2%)	13.2	-13.4	-0.6
300°C	35.7(-14.1%)	35.1(-11.6%)	24.7(-30.2%)	23.6(-23.1%)	-1.5	-30.8	-34.0
400°C	38.3(-7.9%)	38.7(-2.6%)	32.2(-8.9%)	29.1(-4.9%)	1.2	-15.8	-23.8
600°C	37.2(-10.5%)	24.2(-39.1%)	25.8(-27.2%)	24.5(-19.9%)	-34.8	-30.7	-34.1
800°C	15.9(-61.7%)	12.5(-68.5%)	8.6(-75.6%)	8.0(-73.8%)	-21.4	-45.7	-49.6

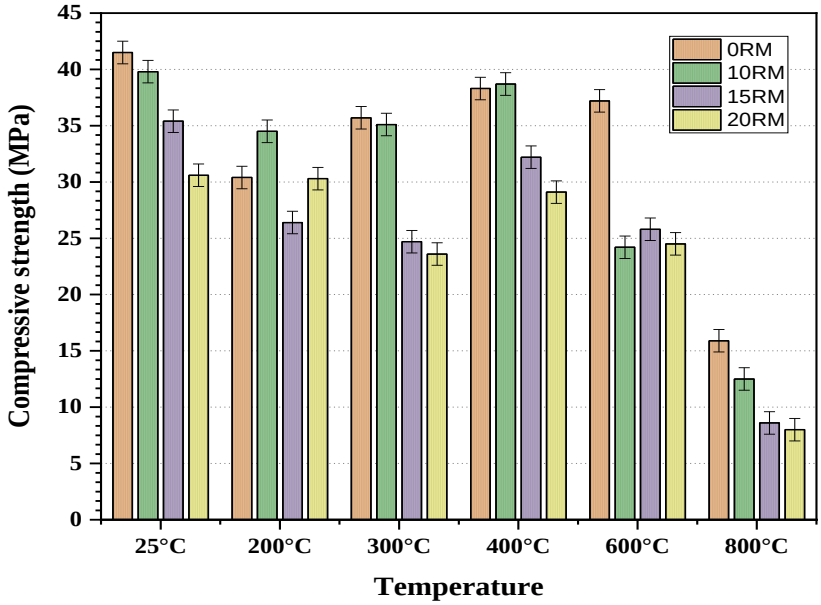

Fig. 4. Compressive strengths of concrete at different temperatures.

Table 9. Splitting tensile strengths of concrete at different temperatures.

	Tensile strength of concrete (MPa) (to their initial 25°C strengths %)				Variation vs. control specimen (%)		
Temperature	0RM	10RM	15RM	20RM	10RM	15RM	20RM
25°C	4.2	4.1	4.2	3.0	-1.9	0.0	-27.9
200°C	3.6(-12.5)	2.7(-33.1)	2.6(-36.7)	2.2(-25.7)	-25.0	-27.6	-38.7
300°C	3.7(-10.0)	2.5(-37.6)	2.1(-48.8)	2.1(-29.5)	-32.0	-43.0	-43.5
400°C	3.3(-19.7)	2.9(-28.9)	2.2(-47.5)	1.6(-46.6)	-13.1	-34.6	-52.0
600°C	1.7(-60.2)	1.5(-62.8)	1.0(-76.3)	0.7(-76.3)	-8.3	-40.5	-57.2
800°C	0.7(-83.8)	0.6(-85.5)	0.5(-88.3)	0.3(-89.5)	-12.3	-27.7	-53.2

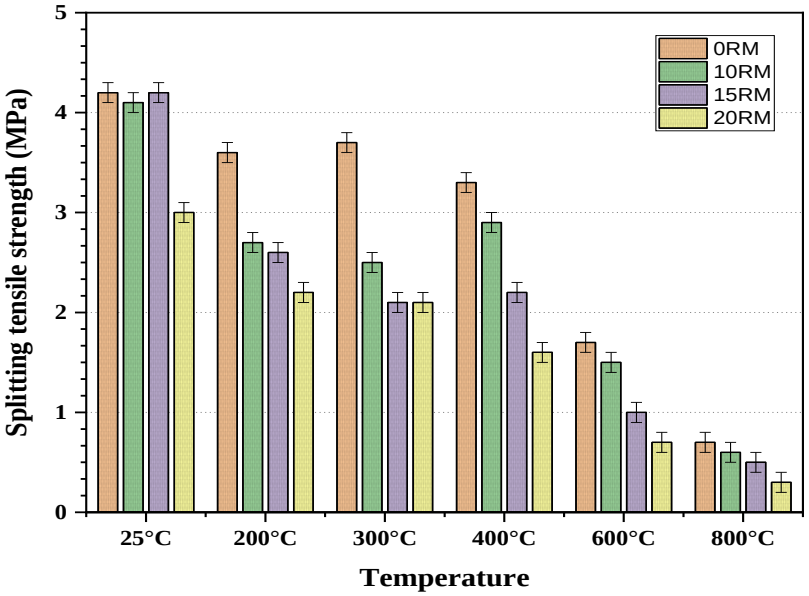

Fig. 5. Splitting tensile strengths of concrete at different temperatures.

3.3. Residual compressive and splitting tensile strengths after heating

In general, compressive strength decreased with the increase in temperature. Fig. 4 and Table 8 show the compressive strength and the decreases in compressive strength compared to 25°C (%), for the concrete samples 0RM, 10RM, 15RM, and 20RM. At 200°C, the compressive strength of all samples decreased by 13–27% with respect to their strength at 25°C, while when compared to the reference specimen (0RM), the 10RM resulted in an increase in compressive strength by 13.2%, whereas 15RM and 20RM resulted in a decrease in compressive strength by 13.4% and 0.6%, respectively. A considerable decrease in compressive strength was noticed in all mixtures after heating to 300°C. This may have been due to more extensive inner cracking of such a compact structure caused by the build-up of pressure that resulted out of the evaporation of physically and chemically bound water (Behnood and Ghandehari, 2009). In general, a small loss in strength was noticed for all of the concretes when exposed to high temperature, while the 10RM group almost was close to the control group and even better results at 400°C. However, the effect of high temperature was more pronounced for concretes with higher RM ratios. More detailed studies are needed to explain the behavior of RM samples, especially at 400°C, where the effect of RM is positive. Likewise, at 600°C, the maximum reduction in compressive strength compared to 0RM took place at 10RM. This strength loss value was largely attributed to the decomposition of calcium hydroxide (Behnood and Ghandehari, 2009). Note that, compared to 0RM, the maximum reduction in compressive strength took place for the 20% red mud mix when exposed to 800°C.

Similar results were obtained for the tensile strengths of the mixes after exposure to different temperatures for a duration of 3h. The tensile strength for different exposure temperatures at a 28-day interval for the 0%, 10%, 15%, and 20% red mud concrete mixes are presented in Table 9 and Fig. 5. The lowest residual tensile strength was observed in 10RM in comparison to 0RM. The tensile strength losses of red mud concrete were low in comparison to the tensile strength losses of the control (0RM) concrete exposed high temperatures.

3.4. Water permeability test (water penetration depth)

Water permeability test provides a measure of a concrete's resistance against penetration of water. Fig. 6 clearly shows the increase in water penetration depth with red mud. The amount of increase in comparison to 0RM was approximately 21%, 42.1%, and 57.9% for 10RM, 15RM, and 20RM, respectively. 10RM provided the lowest water penetration depth value followed by 15RM and 20RM. The effect of the red mud content on permeability could be clearly recognized. The higher content of red mud was related to an increase in the permeability coefficient. The relationship between compressive strength and depth of penetration was linear and is shown in Fig. 7. In general, a very good correlation was observed between water penetration depth and compressive strength values, i.e., as the strength of concrete increased, the water penetration depth decreased significantly. The change in depth of penetration for a given change of red mud content was lower for lower values of RM ratios as a result of the decrease in concrete porosity as the RM ratio decreased. In conclusion, the water permeability test showed that the 10RM concrete provided the lowest water penetration depth value in comparison to 0RM, which ultimately supports the use of red mud as 10%.

3.5. Capillary water absorption test

Capillary water absorption test determines the rate of water absorption through the concrete surface (Zhu and Bartos, 2003; Medeiros and Helene, 2009). Each point on

Fig. 8 is the averaged value of measurements of three specimens. The capillary permeability of the concrete changed depending on the proportion of red mud addition. It may generally be seen that the control concrete exhibited greater resistance to water absorption by capillary suction than the concrete containing red mud, and 10RM provided the lowest absorption value followed by 20RM, whereas the highest absorption value was obtained in 15RM. Moreover, it may be seen in Fig. 8 that the same absorption value could be obtained with 0RM and 10RM (i.e., about 700 and 800 g/m² capillary absorption in 24 h for 0RM and 10RM, respectively). In addition, it was shown that 15RM and 20RM provided the highest absorption values (i.e., about 6800 and 4200 g/m² capillary absorption in 24h for 15RM and 20RM, respectively).

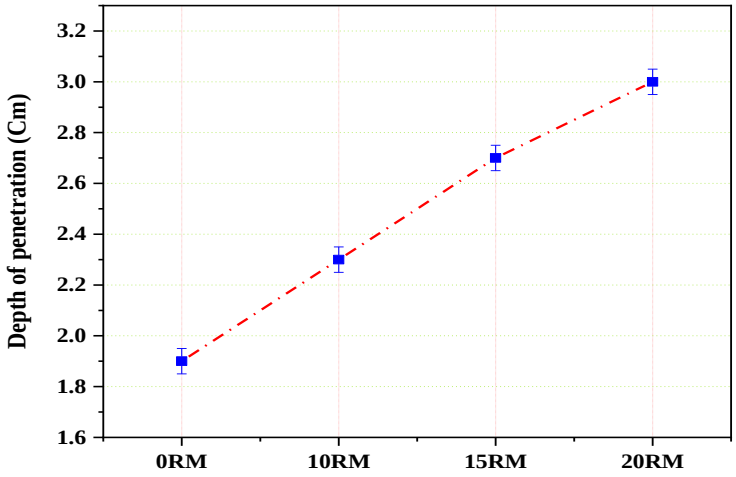

Fig. 6. Permeability test of concrete.

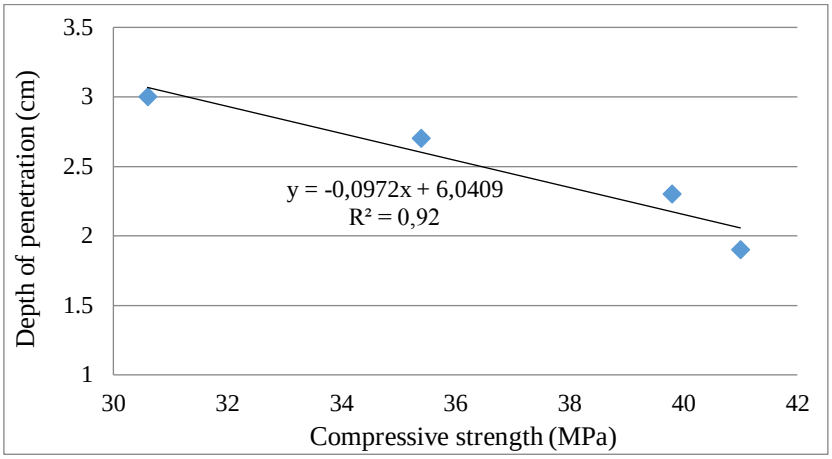

Fig. 7. Compressive strength and depth of penetration relationship.

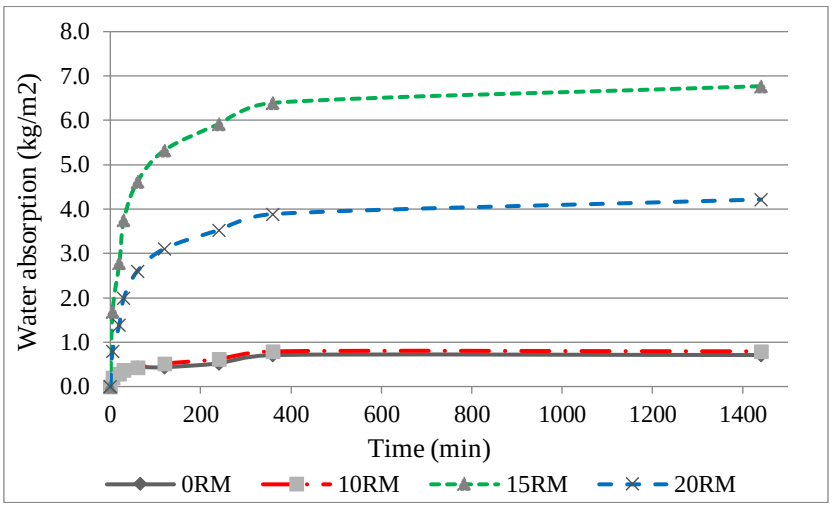

Fig. 8. Capillary water absorption of concrete.

4. Conclusions

The main purpose of this experimental study is to measure the effect of 25, 200, 300, 400, 600, and 800 ° C temperatures for 3 hours. Four mixes with red mud (0%, 10%, 15% and 20%) replacing cement by weight were used to evaluate the residual compressive and tensile strength of concrete as well as weight loss values after high-temperature exposure. Moreover, to study the permeability properties of concrete, capillary water absorption and water permeability tests were performed on all four mixes. The following results were found:

- The weight loss was somewhat higher in the 15RM and 20RM concrete groups in comparison to the control concrete, and this loss was higher especially at a temperature of 300°C.
- From the point of view of compressive strength, the 10RM group almost was close to the control concrete and provided even better results at some temperatures (400°C). However, at higher RM ratios there was a decrease in strength.
- Under high-temperature effect, all mixtures have a marked decrease in their compressive strength when heated to 300°C. At 400°C, however, there was an increase in compressive strength of 10RM and a decrease in higher red mud proportions. More detailed investigations are needed to explain the behavior of RM samples, especially at 400°C, where the effect of RM is positive.
- At higher temperatures (e.g. 600°C), the maximum reduction in compressive strength was observed at 10 RM in comparison to 0 RM. Whereas at 800°C, the maximum reduction in compressive strength was in 20RM.
- In terms of splitting tensile strength, positive results were not obtained in the groups with RM. It is advised to use fibers to increase tensile strength especially when red mud is used.
- The water permeability test showed that the 10RM sample provided the lowest water penetration depth value compared to 0RM, which ultimately supported the use of red mud as 10%.

For further studies,

- Evaluation of the pozzolanic activity of red mud is also required at different ages,
- It is needed to examine the changes in properties with different curing methods and more mineral additive materials,
- The effects of different methods of cooling after high temperature exposure should be examined,
- Detailed microstructure and pore structure studies are recommended on the topic (e.g., MIP, SEM, BET, XRD, TGA) to determine the mechanism of red mud as a partial replacement exposed to high temperature,
- Examination of freeze-thaw and other durability properties is recommended,
- It is advisable to examine the properties of different concrete types with red mud (e.g., high strength concrete and fiber-reinforced concrete) at high temperatures. To increase tensile strength, which is particularly low, different materials (steel fiber, polymer fiber, etc.) could be added to the concrete with red mud.
- Additionally, post-temperature properties should be examined at the sintered state.

References

Alameri I (2017). Atık Kırmızı Çamur ve Nano Al_2O_3 Katkılı Betonların Yüksek Sıcaklık Sonrası Fiziksel ve Mekanik Özelliklerinin İncelenmesi. *MSc thesis*, Atatürk University, Erzurum, Turkey. (in Turkish)

Alameri I, Oltulu M (2019). The effect of high temperatures on the properties of hardened concrete with bauxite residue materials. *Mas International Conference on Mathematics-Engıneering-Natural & Medical Sciences*, Erzurum, Turkey.

Alameri I, Oltulu M, Ardahanlı M (2019). Effect of early-age temperature on the behavior of concrete containing silica fume. *3rd International Conference on Advanced Engineering Technologies*, Bayburt, Turkey.

AlSheikh SA (2011). Mechanical properties for high performance concrete exposed to high temperature. *International Journal of Civil and Structural Engineering*, 2(2), 435–444.

Ardahanlı M, Oltulu M, Alameri I (2019). Evaluation of the mechanical properties of self-compacting concrete containing fly ash subjected to early-age temperature. *Hoca Ahmet Yesevi 2. Uluslararası Bilimsel Araştırmalar Kongresi*, Erzurum, Turkey.

ASTM C1585-13 (2013). Standard Test Method for Measurement of Rate of Absorption of Water by Hydraulic-Cement Concretes. ASTM International, West Conshohocken, PA.

Baradan B, Yazıcı H, Ün H (2010). Beton ve betonarme yapılarda durabilite. Türkiye Hazır Beton Birliği, Turkey.

Beglarigale A, Yalçınkaya Ç, Yigiter H, Yazıcı H (2016). Flexural performance of SIFCON composites subjected to high temperature. *Construction and Building Materials*, 104, 99–108.

Behnood A, Ghandehari M (2009). Comparison of compressive and splitting tensile strength of high-strength concrete with and without polypropylene fibers heated to high temperatures. *Fire Safety Journal*, 44, 1015–1022.

Bishetti PN, Pammar L (2014). Experimental study on utilization of industrial waste in concrete. *International Journal of Technical Research and Applications*, 2(4), 49-52.

DIN 1048-5 (1991). Determination of permeability of concrete. Deutsches Institut für Normung eV, Germany.

Hu W, Nie Q, Huang B, Shu X, He Q (2018). Mechanical and microstructural characterization of geopolymers derived from red mud and fly ashes. *Journal of Cleaner Production*, 186, 799-806.

Kushwaha M, Akhtar S, Rajput S (2013). Development of the self compacting concrete by industrial waste (red mud). *International Journal of Engineering Research and Applications*, 3(4), 539-542.

Liu R, Poon C (2016). Effects of red mud on properties of self-compacting mortar. *Journal of Cleaner Production*, 135, 1170-1178.

Manfroi EP, Cheriaf M, Rocha JC (2014). Microstructure, mineralogy and environmental evaluation of cementitious composites produced with red mud waste. Construction and Building Materials, 67, 29-36.

Medeiros MHF, Helene P (2009). Surface treatment of reinforced concrete in marine environment: Influence on chloride diffusion coefficient and capillary water absorption. *Construction and Building Materials*, 23, 1476–1484.

Metilda DL, Selvamony C, Anandakumar R, Seeni A (2015). Investigations on optimum possibility of replacing cement partially by red-mud in concrete. *Scientific Research and Essays*, 10(4), 137-143.

Nath H, Sahoo P, Sahoo A (2015). Characterization of red mud treated under high temperature fluidization. *Powder Technology*, 269, 233–239.

Oltulu M, Alameri I (2019). The mechanical properties of concrete with red mud (bauxite residue) and nano-Al_2O_3 at high temperatures. *Fresenius Environmental Bulletin*, 28(6), 4692-4701.

Rana AY and Sathe NA (2015). Analysing the potential substitute of red mud in concrete adding lime and silica. *International Journal of Emerging Technology and Advanced Engineering*, 5(4), 410-414.

Rathod RR, Kulkarni PM, Shingade VS, Deshmukh SS (2015). Suitability of red mud as an admixture in concrete. *International Journal of Modern Trends in Engineering and Research*, 4th International Conference on Recent Trends in Engineering and Technology. SNJB's KBJ College of Engineering, Chandwad, Nashik, Maharashtra, India.

Rathod RR, Suryawanshi NT, Memade PD (2014). Evaluation of the properties of red mud concrete. *Journal of Mechanical and Civil Engineering*, Second International Conference on Emerging Trends in Engineering, Dr.J.J. Magdum College of Engineering, Jaysingpu, India.

Ribeiro DV, Labrincha JA, Morelli MR (2010). Use of red mud as addition for portland cement mortars. *Journal of Materials Science and Engineering*, 4(8), 1-8.

Ruano G, Isla F, Luccioni B, Zerbino R, Giaccio G (2018). Steel fibers pull-out after exposure to high temperatures and its contribution to the residual mechanical behavior of high strength concrete. *Construction and Building Materials*, 163, 571-585.

Sancak E, Dursun Sari Y, Simsek O (2008). Effects of elevated temperature on compressive strength and weight loss of the light-weight concrete with silica fume and superplasticizer. *Cement & Concrete Composites,* 30, 715–721.

Sanchayan S, Foster SJ (2016). High temperature behaviour of hybrid steel–PVA fibre reinforced reactive powder concrete. *Materials and Structures*, 49, 769–782.

Sawant AB, Kumthekar MB, Diwan VV, Hiraskar KG (2012). Experimental study on partial replacement of cement by neutralized red mud in concrete. *International Journal of Engineering and Advanced Technology*, 2(1), 282-286.

Tang L (2014). Study of the possibilities of using Red Mud as an additive in concrete and grout mortar. Svensk Kärnbränslehantering AB Swedish Nuclear Fuel and Waste Management Co., Stockholm, Sweden.

Tanyıldızı H, Asiltürk E (2018). High temperature resistance of polymer-phosphazene concrete for 365 days. *Construction and Building Materials*, 174, 741-748.

Torić N, Boko I, Juradin S, Baloević G (2014). Post-fire reductıon of concrete's mechanical properties and its impact on residual load capacity. *8th International Conference on Structures in Fire*, Shanghai, China.

TS EN 196-1 (2016). Methods of testing cement-Part 1: Determination of strength. Turkish Standards Institute, TSE, Ankara, Turkey.

TS EN 197-1 (2012). Cement Part 1: Compositions and conformity criteria for common cements. Turkish Standards Institute, TSE, Ankara, Turkey.

TS EN 206 (2014). Design of concrete mixes. Turkish Standards Institute, TSE, Ankara, Turkey.

TS EN 1097-6 (2013). Specific gravity and water absorption. Turkish Standards Institute, TSE, Ankara, Turkey.

TS EN 12390-3 (2013). Testing hardened concrete–Part 3: Compressive strength of test specimens. Turkish Standards Institute, TSE, Ankara, Turkey.

TS EN 12390-6 (2010). Testing hardened concrete: tensile strength of test specimens. Turkish Standards Institute, TSE, Ankara, Turkey.

Zhu W, Bartos PJM (2003). Permeation properties of self-compacting concrete. *Cement and Concrete Research*, 33(6), 921-926.

Challenge Journal of Concrete Research Letters

Research Article

Influence of nano-modification on mechanical and durability properties of cement polymer anticorrosive coating

Shoib Bashir Wani [a,*], Junaid Ahmed [a], M. S. Haji Sheik Mohammed [a], Tahir Hussain Muntazari [b], Nusrat Rafique [c]

[a] *Department of Civil Engineering, B. S. Abdur Rahman University, Vandalur, Chennai 600048, India*
[b] *Department of Civil Engineering, National Institute of Technology Srinagar, J&K 190006, India*
[c] *Department of Geography & Regional Development, University of Kashmir, J&K 190006, India*

ABSTRACT

In the present study performance evaluation of nano-modified cement polymer anticorrosive coating (CPAC) was undertaken by conducting the Chemical Resistance Test (CRT), Applied Voltage Test (AVT), Bond Strength Test (BST), Accelerated Corrosion Test (ACT) and Coating Flexibility Test (CFT). The site oriented coating comprises of nitrite, styrene-butadiene polymer and other additives. The anticorrosive polymer solution is compatible with concrete or cement when uniformly mixed with fresh ordinary portland cement (OPC). Totally forty-five specimens were subjected to various performance evaluation tests. In CRT observations were made on drilled and undrilled specimens after 45 days test period in liquid and vapour phase. The coating did not blister, soften and lose bond in all the tested medium during CRT and meet the requirement of BIS 13620-1993 and ASTM A775/A775M.The coating has the ability to withstand the electrochemical stresses during one-hour AVT. In the BST, single and double coated rebars showed +126.96% and +46.08% greater usable bond strength respectively than uncoated rebar. In the ACT, there is a significant escalation in time of cracking of specimens of double-coated reinforced rebars by 2 times as compared to uncoated rebars. Cracking time for single coated reinforced rebars was found 1.6 times more than uncoated rebars. In the CFT, coating completely in the inner and the outer radius of the 180° bend rebar fails to meet the requirements of BIS and ASTM standards. Thus the coating has to be applied subsequent to cutting and rebar twisting is finished.

ARTICLE INFO

Article history:
Received 11 June 2020
Revised 22 July 2020
Accepted 12 August 2020

Keywords:
Concrete
Corrosion
Cement polymer anticorrosive coating
Coated rebars
Durability
Uncoated rebars

1. Introduction

The durability problem of concrete structures reinforced with high yield strength deformed (HYSD) rebars is worldwide. Many concrete structures deteriorate prematurely, and repair and maintenance costs amount to substantial proportions of public and private sector budgets. Vishnu et al. (2012) commented as: "In reinforced concrete (RCC), the tensile strength of steel and the compressive strength of concrete work together to allow the member to sustain the stresses over considerable spans. However, failures in concrete structures do still occur as a result of premature reinforcement corrosion". Neville (1987) suggest reasons for "durability problems as poor understanding of deterioration processes, inadequate acceptance criteria of site concrete, and changes in cement properties and construction practices. Nevertheless, the greatest threat to durability of concrete structures is undoubtedly corrosion of embedded reinforcing steel, leading to cracking, staining, and spalling of the cover concrete. This, in turn, can lead to unserviceable structures that may be compromised in respect of safety, stability, and aesthetics". Alekseev et al. (1990) commented on the above scenario as "the durability of reinforcement

* *Corresponding author*. Tel.: +91-962-223-8788 ; E-mail address: shoibbwani@gmail.com (S. B. Wani)
ISSN: 2548-0928 / DOI: https://doi.org/10.20528/cjcrl.2020.04.002

specimens with a stepped (deformed) profile may be roughly an order less than that of smooth specimens since the former have stress concentrators on the surface at the bases of projections, which represent sites of preferential formation of cracks". According to the 2005 report from the Ministry of Shipping, India loses Rs 2,500 crores annually due to corrosion which will be more as of present time.

Gidion Turu'allo (2006) stated that when steel reinforcement is encased in sound dense concrete, the entire surface of the steel is covered by a stable protective oxide film that forms an alkaline environment created by the hydration of the cement in the concrete. Under these circumstances, no corrosion of the reinforcement can occur. However, if the protective oxide film is locally destroyed, for example by the introduction of chloride ions, areas of different potential can be set up on its surface. This difference in potential can result in electrochemical corrosion cells forming between areas on the reinforcement where the protective film has been destroyed and the remainder of the surface where the film is still intact. Such cells create minute electric currents which flow through the reinforcement in one direction and return through the concrete by electrolytic conduction. The areas where the electrons leave the reinforcement to enter the concrete are called anodes and they corroded, whereas the areas where the current re-enters the reinforcement do not corrode and are called cathodes. Corrosion takes place at the anode with metal ions going into solution (refer Eq. (1)).

$$Fe \rightarrow Fe^{++} + 2e^{-} \quad (1)$$

The cathode simply provides the mechanism for the removal of electrons left in the reinforcement by the corrosion process (refer Eq. (2)). Fig. 1 shows the schematic representation of the basic process of corrosion of steel in concrete.

$$O_2 + 2H_2O + 4e^{-} \rightarrow 4OH^{-} \quad (2)$$

Since corrosion is the reaction of a metal with its environment, control can be achieved either through modifications in the metal or the environment. The economy is the overriding factor and for this reason, cheaper and less corrosion-resistant materials are often preferred. Numerous measures have been taken to prevent corrosion of the embedded steel in concrete. In the present study performance evaluation of nano-modified CPAC was undertaken by conducting various mechanical and durability tests. The nano-modification was done by Titanium dioxide (TiO_2).

Fig. 2 shows the scanning electron microscope (SEM) images of the coating.

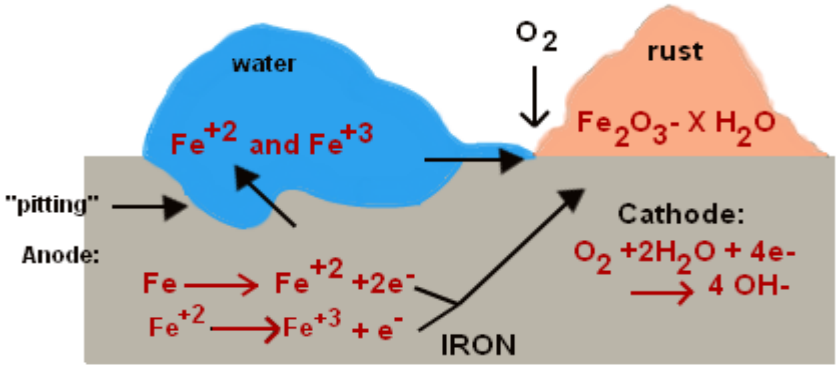

Fig. 1. Schematic representation of process of corrosion of steel in concrete.

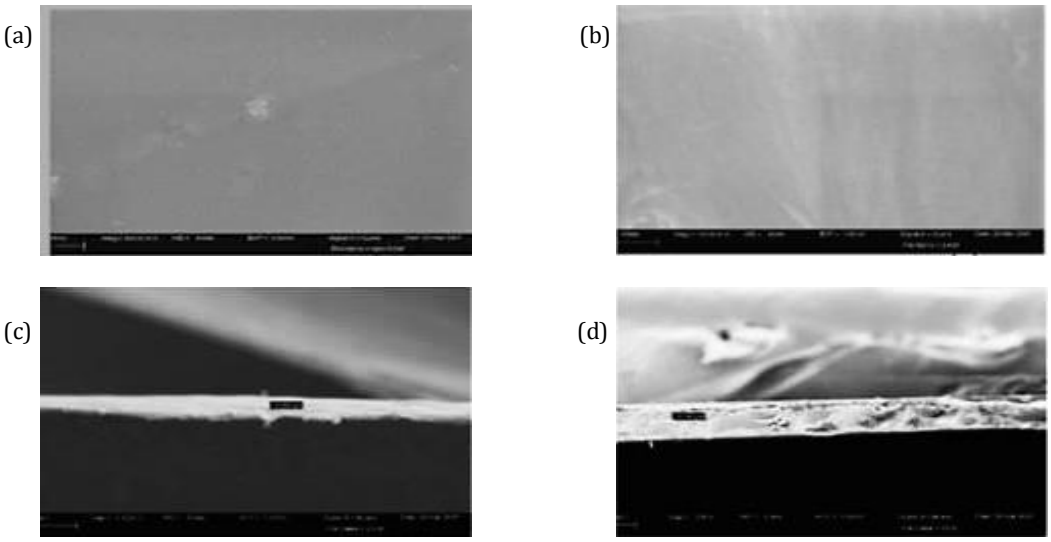

Fig. 2. SEM images of a) Plain CPAC; b) TiO_2 modified CPAC; c) Cross-sectional view of 1coat coating; d) Cross-sectional view of 2-coat coating. All images have a magnification level of approximately 100,000 times.

2. Materials and Material Properties

The materials used for the experimental study include 53 grade OPC approved by BIS 12269 (1987), 20 mm downgraded coarse aggregate (CA), locally available river sand as fine aggregate (FA) of zone II as specified in BIS 383 (1970), potable water, commercially available 12 mm and 16 mm HYSD rebars of grade Fe-500 conforming to BIS 1786 (2008) and nano-modified CPAC.

The basic properties of the cement such as specific gravity, consistency, initial setting time and final setting were found as per BIS 4031-Part 2 and 5 (1988) and the properties of aggregates were found in accordance to BIS 2386-Part 3 (1963). The basic properties of cement, FA and CA obtained and standard values are tabulated in Table 1.

Based on the above material properties, the mix design ratio for M 25 concrete grade was formulated as per BIS 10262 (2009) as shown in Table 2.

The mould, mixing and curing of specimens conform to the requirements as specified in BIS 516 (1959). The average 28 days compressive strength for M25 grade of concrete was recorded as 34.85 MPa. The calculated target mean strength was 31.6 MPa. Therefore the obtained mix design ratio was well within the standard.

Table 1. Properties of cement, fine aggregate and coarse aggregate.

Description	Obtained Value	BIS Recommended Range
Consistency	27 %	> 25%
Initial setting	Minutes	> 30 minutes
Final setting	5 hours and 30 minutes	< 60 hours
Cement - Specific gravity	3.10	-
Fine aggregate - Fineness Modulus	3.05	2.9-3.2
Fine aggregate - Specific Gravity	2.53	2.4-2.6
Coarse aggregate - Fineness Modulus	7.4	6.5 – 7.5
Coarse aggregate - Specific Gravity	2.79	-

Table 2. Design mix proportions for 1m^3 of concrete.

Cement (kg/m^3)	FA (kg/m^3)	CA (kg/m^3)	Water (litre/m^3)
340	643.54	1136.41	186
1	1.89	3.34	0.5

Formulated mix ratio was 1: 1.89: 3.34 and estimated w/c ratio was 0.5.

2.1. Development of nano-modified cement polymer anticorrosive coating system

The nano-modified CPAC on the rebars was applied following BIS 13620 (1993) guidelines. "The site oriented cement polymer anticorrosive coating (passivating type) comprises of nitrite, styrene-butadiene polymer and other additives" as stated by Sheik et al. (2014). The polymer solution is milky white in colour, pH around 12.50 and a density of 1.03 g/cc. This anticorrosive polymer solution is compatible with concrete or cement paste when uniformly mixed with fresh OPC.

The process involves the removal of rust and scales from the steel rebars by hard wire brush and application of coatings by brushing (Shanmugapriya et al., 2015). The nano-modified CPAC was prepared by incorporating 5 gram of Nano Titanium Dioxide (Nano TiO_2) in 1 litre of CPAC. Fig. 3 shows the sequence of the coating process and Fig. 4 shows the view of coated rebars.

3. Experimental Investigation

To evaluate the protective coating on reinforcement rebars, the following criteria were taken into account (Gunaselvi et al., 2015):

- The protective coating should have excellent corrosion-resisting properties.
- The coating should not affect the bond strength of steel to concrete.
- The coating shall withstand the handling stress at the site.

The tests conducted to evaluate the performance of protective coating systems are as under:

- Chemical Resistance Test.
- 2V Applied Voltage Test.
- Bond Strength Test.
- Accelerated Corrosion Test.
- Coating Flexibility Test.

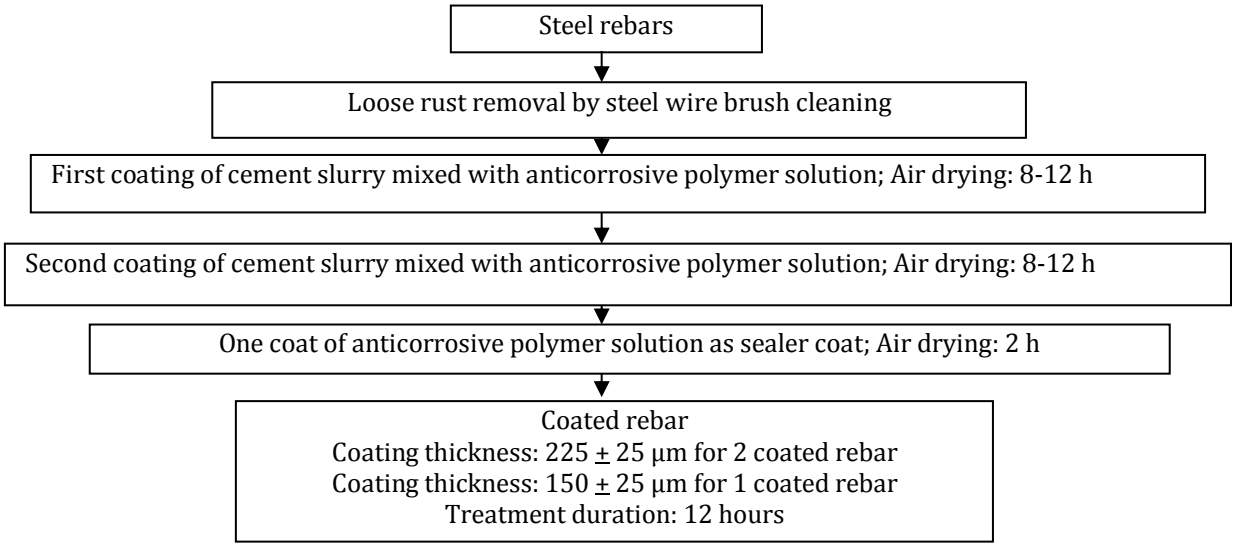

Fig. 3. A sequence of nano-modified cement polymer anticorrosive coating process.

Fig. 4. View of nano-modified cement polymer anticorrosive coated rebars.

3.1. Chemical resistance test

This test was conducted for evaluating the resistance of the coating materials when exposed to various concentrations of reagents. This test was done as per ASTM A775/A775M (1995) and BIS 13620 (1993). Four specimens in CPAC and twelve specimens in Nano TiO_2 modified CPAC were tested. Also, four specimens of Nano TiO_2 modified CPAC with 6mm holidays were tested. In total 20 specimens were tested. The specimens were tested in distilled water, 3M aqueous solution of $CaCl_2$, 3M aqueous solution of NaOH and saturated $Ca(OH)_2$.

Coated rebars of 12 mm diameter and 200 mm length were used. Specimens were positioned vertically in a container and the reagents filled in such a way that the liquid level covers one half of the coated portion. A rubber cork was provided at the bottleneck to prevent the evaporation of the reagents and contamination. Fig. 5 shows the schematic diagram of the chemical resistance test setup.

The test was continued for 45 days at room temperature. After the testing period, the performance of the coating was evaluated based on the blistering, softening, bond loss and development of holes on the rebar surface.

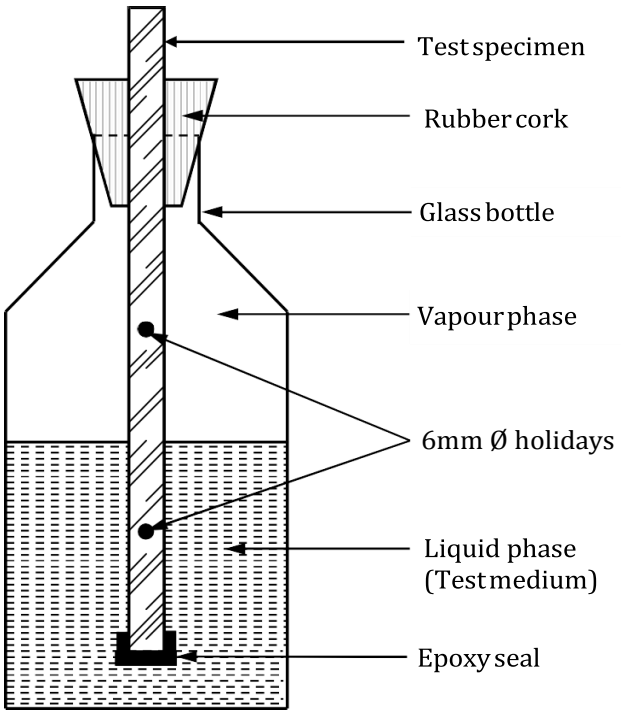

Fig. 5. Schematic view of chemical resistance test setup.

3.2. Applied voltage test

The effects of electrochemical stresses on the bond of coating to steel and film integrity of the coating were assessed by conducting AVT. This is an accelerated type of corrosion test carried out as per BIS 13620 (1993). By varying the thickness of Nano TiO_2 modified CPAC by 2 coats, 3 coats and 4 coats, a total of three specimens were subjected to the test. Coated rebars of 16 mm diameter and 600 mm length have been used.

In the test setup, two numbers of coated rebars, one acts as a cathode and other acts as an anode. Copper wires of 14 mm gauge were clipped at one end of each rebar. The other end of the rebars were sealed with M-seal and coated with an insulation varnish up to a length of 25 mm. The exposed coating surface area on which the test was conducted was restricted to less than 232 cm^2. The remaining exposed area has to be applied with an insulating varnish. A non-conductive plastic container of size 150 mm x 150 mm x 620 mm was used for the test. The container was filled with 7% sodium chloride (70g/lit) solution up to a height of 580 mm. The coated rebars were suspended vertically to have a clearance of 25 mm from the bottom, 40 mm from the sides and 40 mm between the rods. A potential of 2V was impressed for a period 60 minutes between the coated rebars. Fig. 6 shows the schematic diagram of applied voltage test setup.

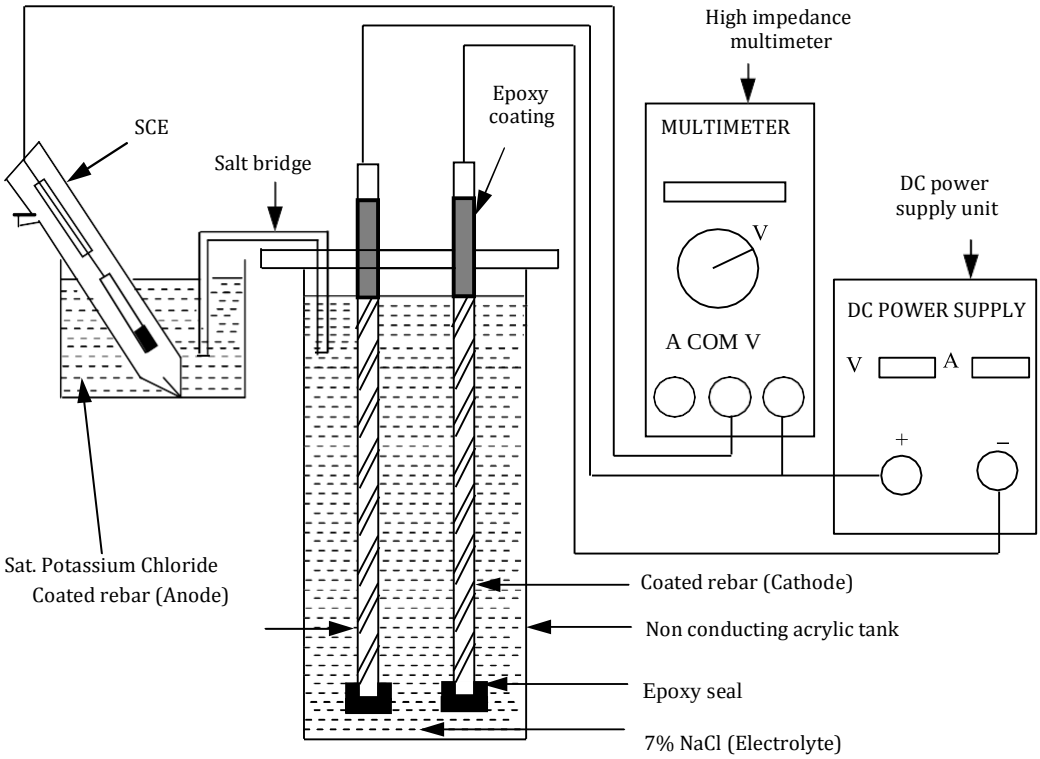

Fig. 6. Schematic view of applied voltage test setup.

A saturated calomel electrode (SCE) with saturated potassium chloride as electrolyte and salt bridge made of agar-agar was used for measuring reference electrode potential. The potential measurements of SCE were observed at every 5 minutes interval during the test period using high impedance multimeter. The current development was also monitored at regular intervals to observe the evaluation of hydrogen gas at the cathode during the test. After the completion of the test, corrosion products of iron at the anode were observed and noted.

3.3. Bond strength

This test has been conducted to find the influence of the protective coating on the bond strength of reinforcement with concrete. Pull out tests were carried out on coated rebars with varying coating thickness and also on uncoated rebars as per BIS 2770 Part I (1997) considering the modifications outlined in BIS 1786 (2008). The test results were compared following BIS 13620 Annexure A-5 (1993).

Totally nine specimens were subjected to the test. Three specimens in control and three specimens each in single and double coated Nano TiO_2 modified CPAC. Concrete cubes of size 150 mm×150 mm ×150 mm were cast with 16 mm diameter HYSD rebars (both coated and uncoated) provided up to 20 mm from the bottom face of the cube. The rebar extended over the top face of the cube by sufficient length to facilitate gripping in the UTM. As per BIS 2770 (1997) and BIS 516 (1959), a helical of 6mm diameter, MS rebar conforming to Grade I of BIS 432 Part I (1982) at 25 mm pitch was provided as reinforcement. To avoid the bond near the loaded end, a plastic sleeve of length 70 mm was provided on the rebar in each specimen. Test specimens were immersed in a curing tank for 28 days. Fig. 7 shows the placement of reinforcement inside the mould.

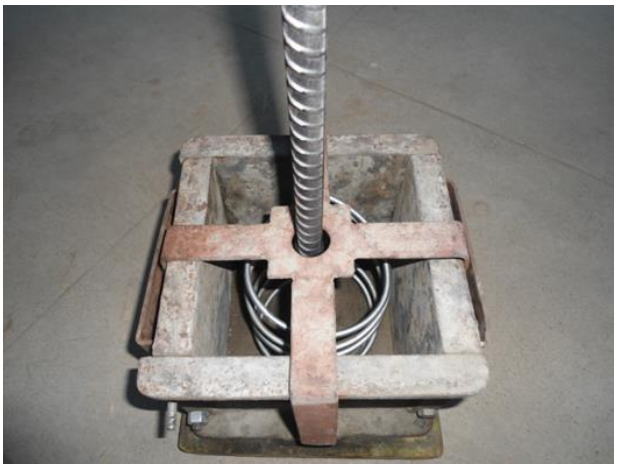

Fig. 7. Placement of reinforcement inside the mould.

The specimens were capped with Plaster of Paris on the loaded end face to obtain a good levelling surface. The load was calibrated with centre hole load cell of 500 kN (Model: ELC-30S) which was placed beneath the loaded end face of concrete cube specimen.

Fig. 8 shows the schematic diagram of the pull-out test setup. Sophisticated dial gauge with a least count of 0.0025 mm was used to measure free end slip and a dial gauge with 0.025mm least count was used to measure loaded end slip. The observation parameters for performance evaluation includes load at 0.025mm free end slip, ultimate failure load, load - slip behaviour at the free end and loaded end and failure mode cum pattern. The load value obtained from 0.025 mm free end slip was used to calculate usable bond strength. Eq. (3) is recommended to calculate bond stresses.

$$u = F/\pi\, dr\, lr \tag{3}$$

where F is the force in rebar, dr is the diameter and lr is the bond length of the rebar. Since the test specimen was provided with helical spring reinforcement, failure pattern was pull-out of rebar instead of a concrete failure by splitting.

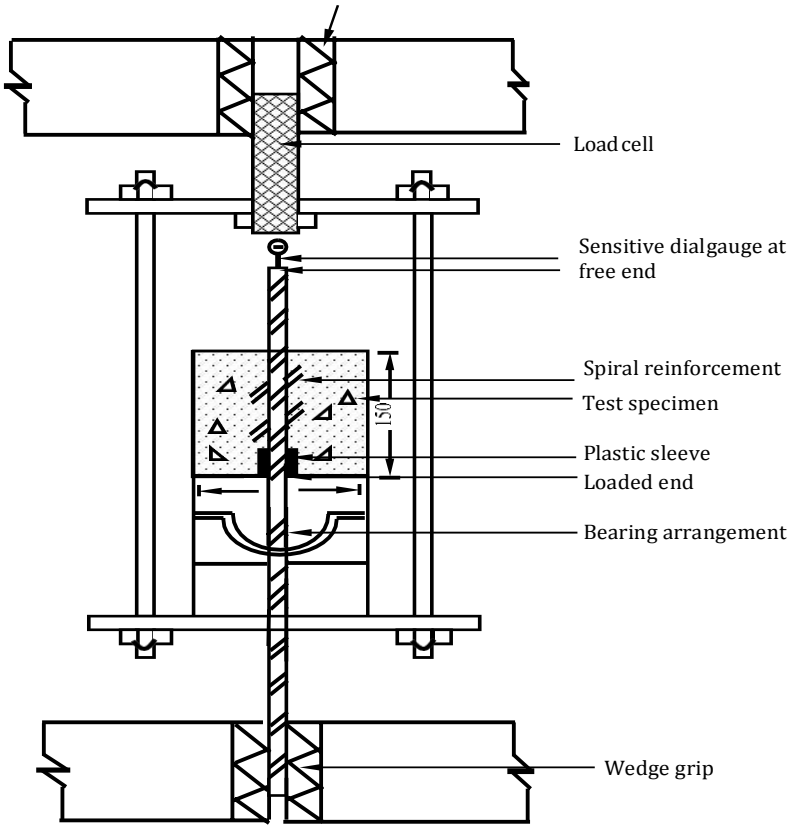

Fig. 8. Schematic view of pull-out test setup.

3.4. Accelerated corrosion test

The accelerated corrosion test (ACT) was conducted to evaluate the resistance of uncoated and coated rebars in enhanced electrochemical corrosion medium. "The test was carried out as per the procedure prescribed by the Structural Engineering Research Centre (SERC), Chennai, India and Central Electrochemical Research Institute (CECRI), Karaikudi, India" (Gunaselvi et al., 2015). Total of nine specimens were subjected to ACT including three control specimens, three specimens each in 1coat and 2coated Nano TiO_2 modified CPAC. The 16 mm diameter and 120 mm long test rebars were centrally embedded in concrete specimens of 70 mm diameter and 115 mm height giving bottom cover as 20mm. The embedded rebar projected 25 mm above the concrete cylinder and it acts as an operational electrode. The bottom portion of the rebar was masked with M-seal and the top portion was faced and clipped with 14 mm copper wire gauge. Also, the specimen was sealed from top and bottom by

polymer cementitious coating to ensure chloride intake from the lateral surface of the specimen.

The container which acted as cathode/counter electrode was filled with 3% NaCl up to the height of the specimen. Anode and cathode were joined to a constant potential of 9V DC supply. The time of appearance of the first crack was adopted to measure the comparative coating resistance against chloride intake and successive deterioration. Fig. 9 shows the schematic diagram of an ACT.

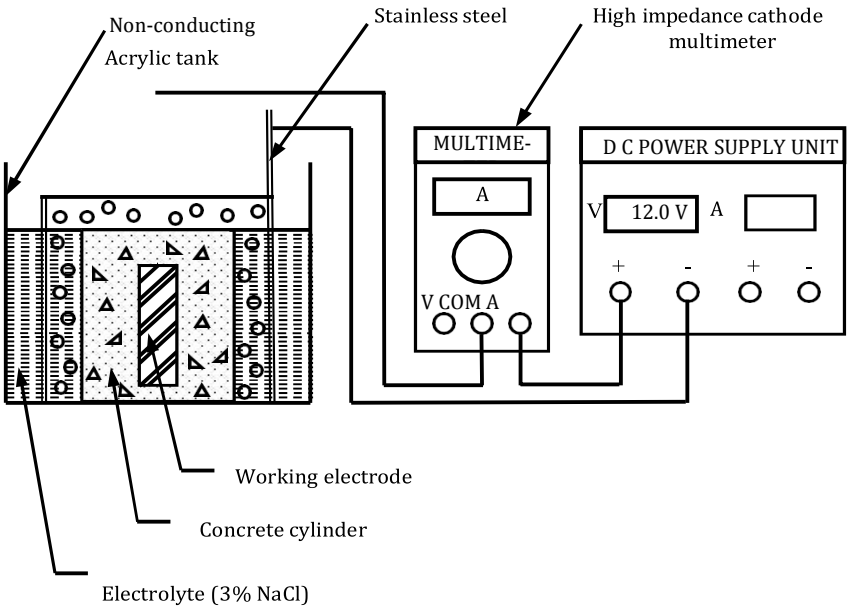

Fig. 9. Schematic view of accelerated corrosion test setup.

3.5. Coating flexibility test

Reinforcement rods are subjected to cutting, bending and shaping operation before they are laid in concrete. To resists these mechanical stresses, the coating should exhibit good flexibility characteristics. Coating flexibility test (CFT) was done as per BIS 13620 Annexure A-4 (1993) and ASTM A775/A775M (1995). The coated rebars of 16 mm diameter and 1 m length were used in the test. The coated rebar was positioned in bar bending arrangement such that the longitudinal ribs and the mandrel radius are in 90° planes. "The rebars were bent around 150 mm diameter mandrel to 180° after a rebound with suitable levers. Thermal equilibrium of 240+20°C was maintained during the test". Fig. 10 shows the CFT test setup.

Fig. 10. Coating flexibility test in progress.

4. Results and Discussion

Totally forty-five specimens were subjected to various performance evaluation tests. The performance of the coated rebars has been evaluated by conducting the following test and it has been discussed.

- Chemical Resistance Test.
- 2V Applied Voltage Test.
- Bond Strength Test.
- Accelerated Corrosion Test and
- Coating Flexibility Test

4.1. Chemical resistance test

Tables 3 and 4 show the observation on CRT for specimens coated with CPAC and nano-modified CPAC. No rust spots were observed in distilled water, 3M sodium hydroxide and saturated calcium hydroxide mediums. In

3M calcium chloride medium, only few rust spot at the interface were observed. The occurrence of rust spot in 3M calcium chloride may be due presence of weak spots in the coating and also due to reduced coating thickness, particularly in ribbed areas.

Table 5 shows the observation on CRT for specimens with holidays. Only in 3M calcium chloride medium few rust spots were observed in both liquid and vapour phase. In all other mediums, no rust spots were observed. The coating did not blister, soften, loss bond in all mediums during the test period. The coating surrounding the intentionally made holes exhibit no undercutting during the 45 days test period in all the medium. Fig. 11(a) shows the view of coated rods immersed in 3M $CaCl_2$ after test period and Fig. 11(b) shows the view of the drilled specimen after subjected to the CRT.

Table 3. Observation on chemical resistance test 1.

S. No.	Medium	Observation on coating	
		Liquid phase	Vapour phase
1	Distilled water	No blistering, softening, disbondment, decolourisation and rust spots	No blistering, softening, decolourisation, disbondment and rust spots
2	Sat. $Ca(OH)_2$	No blistering, softening, decolourisation, disbondment and rust spots	No blistering, softening, decolourisation, disbondment and rust spots
3	3M NaOH	No blistering, softening, discolourisation, disbondment and rust spots	No blistering, softening, decolourisation, disbondment and rust spots
4	3M $CaCl_2$	No blistering, softening, decolourisation and disbondment. Rust spots at the interface	No blistering, softening, decolourisation, disbondment and rust spots

Coating: Cement polymer anticorrosive coating. Test duration: 45 days. Test temperature: 27°C.

Table 4. Observation on chemical resistance test 2.

S. No.	Medium	Observation on coating	
		Liquid phase	Vapour phase
1	Distilled water	No blistering, softening, disbondment, decolourisation and rust spots	No blistering, softening, decolourisation, disbondment and rust spots
2	Sat. $Ca(OH)_2$	No blistering, softening, decolourisation, disbondment and rust spots	No blistering, softening, decolourisation, disbondment and rust spots
3	3M NaOH	No blistering, softening, decolourisation, disbondment and rust spots	No blistering, softening, decolourisation, disbondment and rust spots
4	3M $CaCl_2$	No blistering, softening, decolourisation and disbondment. Rust spots at the interface.	No blistering, softening, decolourisation disbondment and rust spots

Coating: TiO_2 modified cement polymer anticorrosive coating. Test duration: 45 days. Test temperature: 27°C.

Table 5. Observation on chemical resistance test 3.

S. No.	Medium	Observation on coating	
		Liquid phase	Vapour phase
1	Distilled water	No undercutting of the film around the intentional damage.	No undercutting of the film around the intentional damage.
2	Sat. $Ca(OH)_2$	No undercutting of the film around the intentional damage.	No undercutting of the film around the intentional damage.
3	3M NaOH	No undercutting of the film around the intentional damage.	No undercutting of the film around the intentional damage.
4	3M $CaCl_2$	No undercutting of the film around the intentional damage.	No undercutting of the film around the intentional damage.

Coating: TiO_2 modified cement polymer anticorrosive coating with holidays. Test duration: 45 days. Test temperature: 27°C.

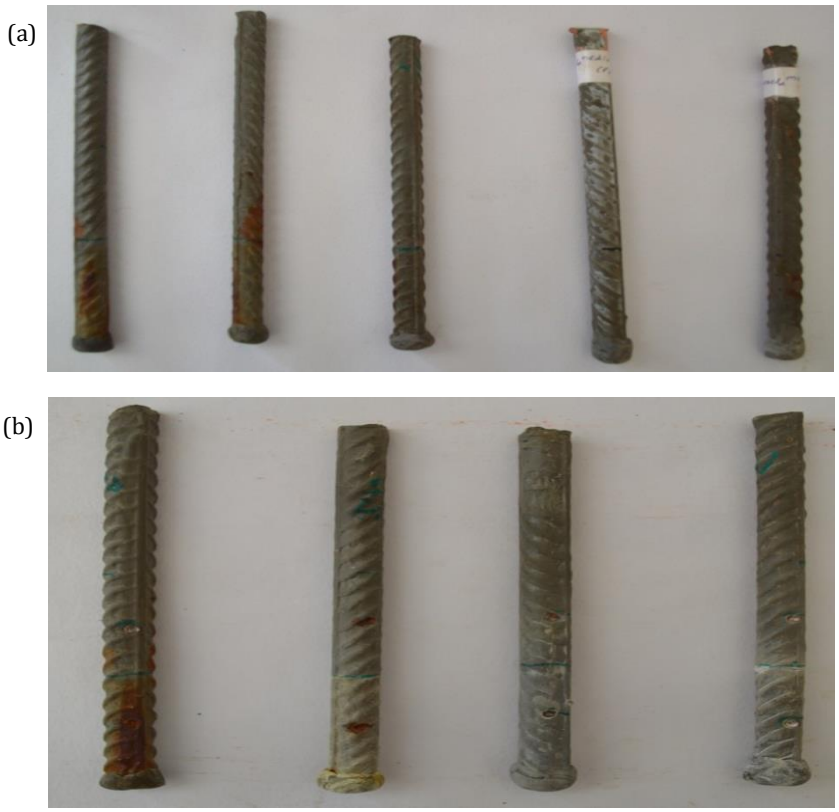

Fig. 11. (a) View of coated specimen immersed in 3M $CaCl_2$ medium after the test; (b) View of drilled specimen after subjected to the chemical resistance test.

4.2. Applied voltage test

The duration of the AVT was one hour. The potential was developed by a D.C power supply of capacity 0-30 Volts. The coating failure was evident by the evaluation of hydrogen gas at the cathode or the appearance of corrosion products of iron at the anode. It was noticed that when a potential of 2V is applied between the coated rebars, there is a steep increase in potential from the open circuit in a 7% NaCl medium. There was no current development during the test period. Table 6 shows the observation of AVT.

Table 6. Observation on applied voltage test for nano-modified CPAC.

Voltage applied	Type of coating	Anode (at the end of test)	Cathode (during the test period)
2.0 Volt (7% NaCl)	Double Coat	Severe corrosion products of Iron.	No evaluation of Hydrogen gas.
	Triple Coat	Two to three corrosion products of Iron	No evaluation of Hydrogen gas.
	Four Coat	No Corrosion Products of Iron.	No evaluation of Hydrogen gas

Table 6 shows that in a double-coated specimen, there was no evaluation of hydrogen gas at the cathode and few rust spots at the anode have been observed. In triple coated specimen, there was no evaluation of hydrogen gas at the cathode and two to three rust spots have been observed in the anode. In four coated specimen, there was no evaluation of hydrogen gas at the cathode and no rust spot at the anode. Fig. 12(a) shows potential vs time behaviour of double, triple and four coated Nano TiO_2 modified CPAC rebar.

For double-coated rebar, there was an increase in potential values of 0.682V observed immediately upon impressing 2V from Open Circuit Potential of - 0.386 mV. Afterwards, there is a similar potential value until the end of the test period. For triple coated rebar there was an increase in potential values of 1.482 mV observed immediately upon impressing 2V from Open Circuit Potential of - 0.192 mV. It was observed that there was a decrease in potential value for 5 minutes and afterwards there is a similar potential value until the end of the test period. For four coated rebar there was an increase in potential values of 2.282 mV observed immediately upon impressing 2V from Open Circuit Potential of - 0.082 mV. It was observed that there was a decrease in potential value for the first 10 minutes and afterwards there was a similar potential value until the end of the test period. Fig. 12(b) shows the coated rebars after subjected to AVT.

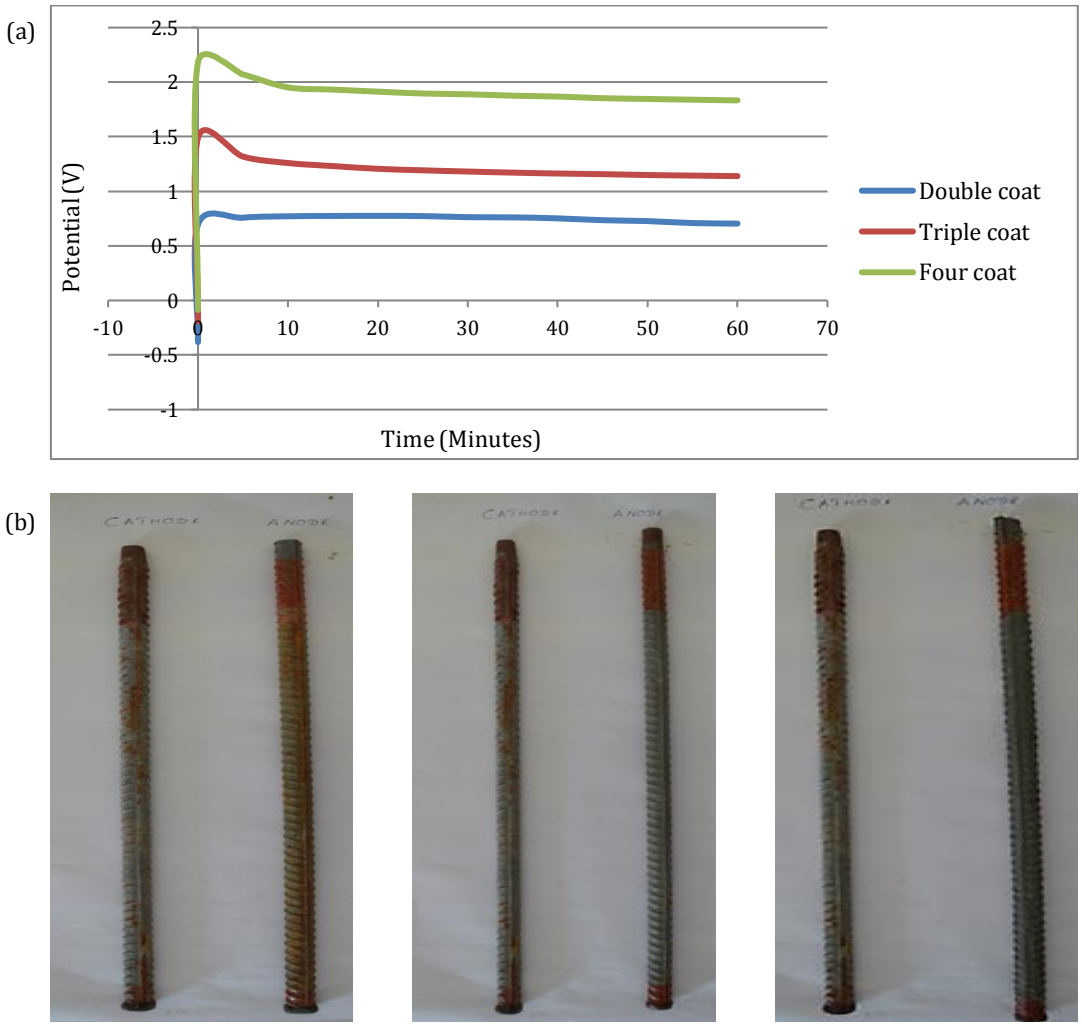

Fig. 12. (a) Potential vs time behaviour of double, triple and four coated Nano TiO_2 modified CPAC rebar; (b) Two, three and four coated specimen after subjected to applied voltage test.

4.3. Bond strength test

The bond strength results of rust-free uncoated rebar were compared with Nano TiO_2 modified CPAC (single and double coating) rebars. The 0.025 mm FE slip was considered for evaluating usable bond strength. Table 8 shows the mean results of pull-out tests for coated and uncoated bars. It was observed that the ultimate load-carrying capacity of nano-modified CPAC single and double coated rebars were 94 kN and 84.32 kN respectively. However, for uncoated rebar, the ultimate load-carrying capacity was 70 kN. From the values, it is observed that single and double coated rebar carries more than 34.29% load and 20.46% load respectively when compared to uncoated rebars. Usable bond strength for single coated rebar is 126.96% and double-coated rebar is 46.08% more when compared to uncoated rebars. Single coated rebar shows better results than double-coated rebar in both load-carrying capacity and usable bond strength. Table 7 shows the BST results.

Fig. 13 shows load vs slip behaviour of 16 mm diameter uncoated and nano-modified cement polymer anti-corrosive coated rebars.

Table 7. Observation on bond strength test for uncoated, single and double coated nano-modified CPAC.

S. No.	Type of Rebar	Load (kN)			Usable Bond Strength (MPa)	Variation (%)
		0.025mm FE slip	0.25mm LE slip	Ultimate Load (kN)		
1	Uncoated rebar	9.25	3	70	2.3	-
2	Single coated CPAC rebar	21	8.5	94	5.22	+126.96
3	Double coated CPAC rebar	13.5	4.75	84.32	3.36	+46.08

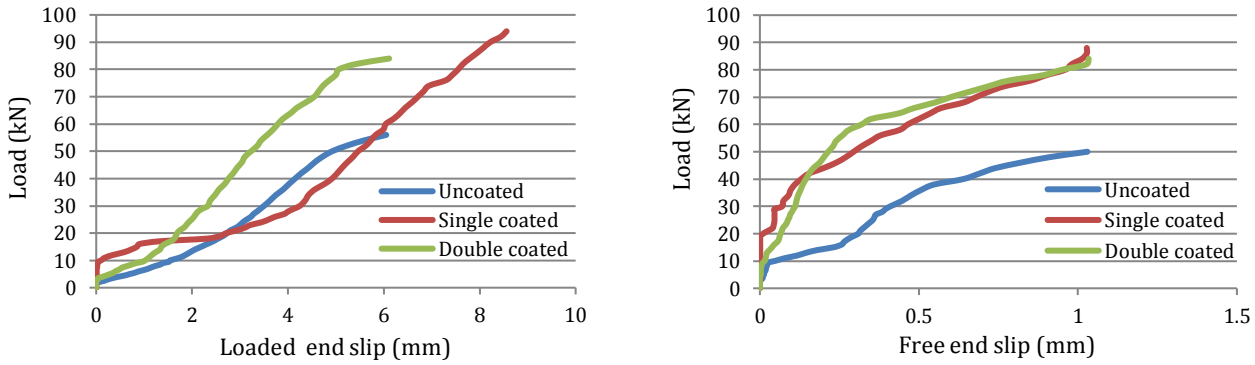

Fig. 13. Load-slip behaviour of 16 mm diameter uncoated and nano-modified CPAC rebars.

4.4. Accelerated corrosion test

Fig. 14(a) shows the comparison of cracking time for uncoated and (single and double) coated rebars in control concrete. It was observed that for all the coated rebars, time to cracking was higher when compared to uncoated control rebars. There was an appreciable increase in cracking time for double-coated Nano TiO_2 modified cement polymer anticorrosive coated rebars of the order of 2 times as compared to uncoated rebars. Cracking time for single coated Nano TiO_2 modified cement polymer anticorrosive coated rebar was 1.6 more than uncoated rebar.

Fig. 14(b) shows the condition of cracked specimens after completion of ACT. The specimens were broken open and observations were noted. Fig. 14(c) shows the condition of the coated rebar and concrete at the end of the test. It was observed that the uncoated rebars were corroded more and the coating is more adhesive to the concrete than rebar.

4.5. Coating flexibility test

Three specimens of nano-modified CPAC rebars were subjected to CFT. It was noticed that for the specimen subjected to the test, cracking and disbondment of the coating was observed on both outside and inside radius of the 180° bent rebar. According to BIS and ASTM codal provisions, no cracking of the coating shall be visible to a person with a normal or corrected vision on the outside radius of 180° bend rebars. Therefore the coating has to be applied after cutting and bending operation is over.

(a)

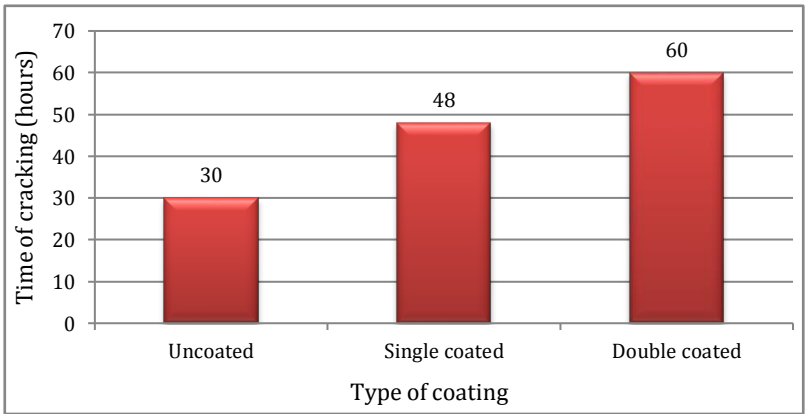

(b)

Uncoated Single coated Double coated

Fig. 14. (continued)

(c)

Fig. 14. (a) Comparison of cracking time for nano-modified CPAC coated (single and double) and uncoated rebar in control concrete; (b) Cracked specimens (uncoated, single and double coated) after subjected to accelerated corrosion test; (c) Condition of concrete and coated rebar at the end of accelerated corrosion test.

5. Conclusions

In the study performance evaluation of nano-modified Cement Polymer Anticorrosive Coating (CPAC) was undertaken by conducting the Chemical Resistance Test (CRT), Applied Voltage Test (AVT), Bond Strength Test (BST), Accelerated Corrosion Test (ACT) and Coating Flexibility Test (CFT). Totally, forty-five specimens were tested to evaluate the performance of the coating. Based on the test results, the following conclusions were drawn:

- The coating did not blister, soften, lose bond in all the tested medium during the chemical resistance test and meets the requirement of BIS 13620 (1993) and ASTM A775/A775 M (1995).
- The coating has the ability to withstand the electrochemical stresses during one hour applied voltage test and passes the Indian standard code requirements.
- The results of the pull-out showed that the usable bond strength for single coated rebar is 126.96% and double-coated rebar is 46.08% more than uncoated rebars. Single coated rebar shows better results than double-coated rebar in both load-carrying capacity and usable bond strength.
- In accelerated corrosion test there is an appreciable increase in cracking time for double-coated Nano TiO_2 modified cement polymer anticorrosive coated rebars of the order of 2 times as compared to uncoated rebars. Cracking time for single coated Nano TiO_2 modified cement polymer anticorrosive coated rebar was 1.6 more than uncoated rebar.
- In the CFT, coating completely in the inner and the outer radius of the 180° bend rebar fails to meet the requirements of BIS and ASTM standards. Therefore the coating must be applied subsequent to cutting and rebar twisting is finished.
- Overall from the test results, it can be concluded that the TiO_2 modified cement polymer anti-corrosive coating offers appreciable corrosion resistance properties, satisfying the codal requirements in critical aspects and therefore can increase the durability of RCC structures several folds.

REFERENCES

Alekseev SN, Ivanov FM, Modry S, Shiessel P (1990). Durability of reinforced concrete in aggressive media. Oxford & IBH Publishing Co. Pvt. Ltd., New Delhi, 1993. (Translation of Dolgovechnosti Zhelezobetonav Agressivnikh Sredakh, Stroiizdat, Moscow, 1990)

ASTM A775/A775M (1995). Standard Specification for Epoxy-Coated Reinforcing Steel Bars. Annual book of ASTM Standards, Vol.01.04.

BIS 383 (1970). Specification for coarse and fine aggregates from natural sources for concrete (Second Revision). Bureau of Indian Standards, New Delhi, India.

BIS 432-Part 1 (1982). Specifications for Mild Steel and Medium Tensile Steel Bars and Hard-Drawn Steel Wire for Concrete Reinforcement. Bureau of Indian Standards, Manak Bhawan 9, New Delhi, India.

BIS 516 (1959).Method of Tests for Strength of Concrete. Bureau of Indian Standards, Manak Bhawan 9, New Delhi, India.

BIS 1786 (2008). Specification for high strength deformed steel bars and wires for concrete reinforcement. Bureau of Indian Standards, New Delhi, India.

BIS 2386 (1963). Methods of test for aggregates for concrete–Part 3: Specific gravity, density, voids, absorption and bulking.

BIS 2770 (1997). Method of testing bond in reinforced concrete part-I. Bureau of Indian Standards, New Delhi, India.

BIS 4031-Part 2 and 5 (1988). Part-2: Methods of physical tests for hydraulic cement, Part-5: Determination of initial and final setting times. Bureau of Indian Standards, New Delhi, India.

BIS 10262 (2009). Recommended guidelines for concrete mix design. Bureau of Indian Standards, New Delhi, India.

BIS 12269 (1987). Specification for 53 grade ordinary portland cement. Bureau of Indian Standards, New Delhi, India.

BIS 13620 (1993). Fusion Bonded Epoxy-Coated Reinforcing Bars – Specification. Bureau of Indian Standards, New Delhi, India.

Cti Technical Note 1 (2013). Corrosion of Steel Reinforcement in Concrete. Cti Consultants Pty Ltd, Abn 56 003 824 815.

Gull S, Wani SB, Amin I (2020). The influence of rib configuration on bond strength development between steel and concrete. *Journal of the Civil Engineering Forum*, 6(1), 193-200.

Gunaselvi S, Pazhani KC (2015). Corrosion control of steel rebars using electroless nickel coating. *Transactions of the Indian Institute of Metals*, 69(4), 859–868.

IS 516 (1959). Method of Tests for Strength of Concrete. Bureau of Indian Standards, Manak Bhawan 9, New Delhi, India.

Mohammed MSHS, Raghavan RS, Knight GMS, Murugesan V (2014). Macrocell corrosion studies of coated rebars. *Arabian Journal for Science and Engineering* 39, 3535–3543.

Neville AM (1987). Why we have concrete durability problems. *Katherine and Bryant Mather International Conference on Concrete Durability*, ACI SP-100, American Concrete Institute, Detroit, 21-48.

Shanmugapriya S, Rajendran S, Joany RM, Sharmila A, Devadharshini K, Sangeetha P, Prabhakar P (2015). Recent trends in studies on corrosion resistance of steel in simulated concrete pore solutions. *International Journal of Nano Corrosion Science and Engineering*, 2(4), 10-20.

Turu'allo G (2006). Corrosion rates measurements by linear polarisation and AC impedance techniques using different steel bars and acidic solution. *SMARTek*, 4(3).

Vishnu JR, Sharma UK (2012). Influence of pre-load on corrosion vulnerability of reinforced concrete. *Advances in Structural Engineering*, 15(7), 1115–1124.

Challenge Journal of Concrete Research Letters

Research Article

An investigation on the properties of woodcrete exposed to high temperature

Mehmet Canbaz [a,*], İlkay Kara [a], İlker Bekir Topçu [a]

[a] *Department of Civil Engineering, Eskişehir Osmangazi University, 26480 Eskişehir, Turkey*

ABSTRACT

By combining wood wastes with various binders, construction materials can be produced. These materials can be used in non-bearing parts such as wall block, insulation panel. In this study, prismatic specimens were taken from the mixtures produced considering the chip-cement ratio as 0.25, 0.5 and 1. The unit weight, ultrasonic pulse velocity, bending and compressive strengths of the specimens were determined by using the results of the experiments on these specimens. In addition, specimens were kept at 200 and 400°C for 3 hours in order to determine its behavior under high temperature, which is one of the most important problems for wood composites. With the experiments carried out on the cooled specimens, weight and strength losses, changes in ultrasonic pulse velocity were examined. As a result of the study, while determining that the chip-cement ratio can be used as 1, it is recommended to use the chip-cement ratio up to 0.5 when the high temperature effect is taken into consideration.

ARTICLE INFO

Article history:
Received 2 May 2020
Revised 21 July 2020
Accepted 31 August 2020

Keywords:
Woodcrete
Chip-cement ratio
High temperature
Mechanical properties

1. Introduction

Studies for the disposal of wastes generated by the increasing industrial activities in today's technology maintain their importance (Mengeloğlu and Alma, 2002). Depending on the type of the wood, up to 2% sawdust waste can be formed from the processing of wood. A very small part of these wood waste is collected by recycling companies. Some of it is used for heating, some is thrown away (Ateş, 2018). As seen in Fig. 1, sawdust is used as recycling in the production of chipboard and medium density fiberboard (MDF).

In recent years, wood-cement-based composites have been preferred in many countries as environmentally friendly and renewable products in order to reduce the cost of materials in construction works, as seen in Fig. 2 (Şahin, 2019). Wood composites are divided into two main classes; wood composites produced with thermoset adhesives are woodcrete produced with materials such as thermoplastic and cement (Aigbomian and Fan, 2013). The low-density ones of Portland cement composites are made of wood wool and the higher-density ones are made of chip or fiber (Ulusoy and Peker, 2019). Cemented particle boards, one of the cemented wood composites, are defined according to the type, shape, color and surface condition of the cement used in the EN 633 standard (EN 633, 1993). The compatibility of cement with wood is high (Wang, 2018). The fact that cement does not require extra additives for hardening unlike other binders in wood composites makes the products obtained more economical (Aras et al., 2019). Although woodcrete is heavier than resin bonded wood composites, it is lighter than concrete (Jorge et al., 2004; Şahin et al., 2019). Wood-cement composites are also more workable, resistant to water, burning, and rotting than other wood composites (Aras and Kalaycıoğlu, 2016). Woodcrete is also resistant to insects (İstek and Gencer, 2014). Woodcrete has been found to be highly resistant to weather conditions and has no significant changes in dimensional changes (Wolfe and Gjinolli, 1996; Kaya, 2020). It is seen that due to the lignocellulosic material it contains, it has a high sound and more importantly heat insulation (Wei and Tomita, 2001; Kalaycıoğlu et al., 2012). The effects of water-cement ratio, cement-chip

* *Corresponding author*. Tel.: +90-222-239-3750 ; Fax: +90-222-239-3613 ; E-mail address: mcanbaz@ogu.edu.tr (M. Canbaz)
ISSN: 2548-0928 / DOI: https://doi.org/10.20528/cjcrl.2020.04.003

"ratio and chip type on woodcrete properties are great (Onursal, 1996). In addition, the type of tree from which the chip is obtained is also important (Risbrudt et al., 2010). For example, the wood species being hardwood and softwood affects strength (Na et al., 2014). Not all tree species are equally suitable for obtaining woody building material using cement and chips. Because some tree species delay the setting of cement. Here, water-soluble sugars and phenols in the structure of the chips are effective in the process of setting (Bozkurt, 1982; De la Gree et al., 2014; Miller and Moslemi, 2007). Chip is used as both aggregate and reinforcement material in wood-cement composite production. It is important that the cement used as binder completely surrounds the chip (Simatupang and Geimer, 1990).

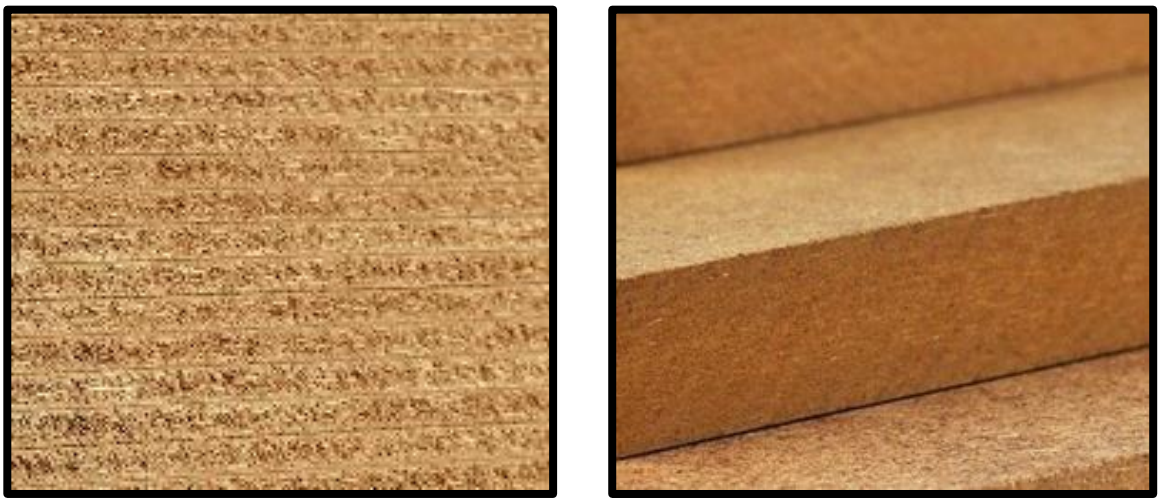

Fig. 1. Partial board and MDF samples.

Fig. 2. Wood-cement based composite specimens.

Although wood waste can be used in the production of wood composites with different resins, mass production of such composites requires a high cost investment. However, since cemented wood composites are easier to produce and their investment costs are lower, a facility to be established where woodworking companies are together has a high potential to transform the waste of these companies into cemented wood composite products. As can be seen from the studies carried out, these products are used as insulation materials due to their lightness and low sound and heat conductivity. Its cement-based nature prevents the wood from being easily flammable. In addition, plasters made on these products make these products more resistant to fire. However, the purpose of this study is to determine the effect of the high temperature that will occur during the fire on the cement-based wood composite properties, unlike other studies. Specimens produced by choosing different ratios of chip-cement were kept at temperatures reaching 400°C and weight and strength losses were determined.

2. Experimental Study

2.1. Materials

The chips shown in Fig. 3, which are the waste of a woodworking company, were used in the study. This company uses Russian fired pine from the Siberian region called North Saphire 117 as its raw material. The unit weight of the chips has been determined as 50 kg/m^3 and its granulometry is given in Table 1. Tap water was used as mixing water and its properties are shown in Table 2. CEM I 42.5 R Portland cement was used as binder and its properties are given in Table 3.

Table 1. Granulometry of pine chips.

Sieve size, mm	16	8	4	2	1
Granulometry, %	100	77	18.4	5.7	0

Table 2. Properties of mixing water.

Chemical Property, mg/l						Physical property	
Al	0.04	Cu	0.016	Ni	5.07	Conductivity, µS/cm	628
NO_3	11.1	Fe	0.007	K	6.8	Hardness, Fd^0	30.11
NH_4	0.06	Mn	0.015	As	1.19	pH	7.35

Table 3. Properties of cement.

Chemical properties				Physical properties	
SiO_2	19,2	K_2O	0,63	Density, g/cm^3	3.09
Al_2O_3	4,56	Na_2O	0,31	Specific surface, cm^2/g	3190
Fe_2O_3	3,09	SO_3	3,21	Setting Time(initial), min	163
CaO	62,9	CI-	0,01	Setting Time(final), min	228
MgO	1,88	LOI	3,8	Expansion, mm	1

Fig. 3. The chip used in the production of woodcrete.

2.2. Method and tests

The chips used as filler in woodcrete production were obtained by mixing with cement paste. Water-cement ratio was kept constant at 0.50 in production. Three different mixtures were made with a chip-cement ratio of 0.25, 0.5 and 1. 4x4x16 cm prismatic specimens were taken from the produced woodcrete mixes and removed from the mold after 1 day and placed in a standard curing environment. Some of the specimens that gained their strength for 28 days were kept at 200°C and some were kept at 400°C for 3 hours according to TS EN 1363-1 (2013) after the oven reached the desired temperature. Left to cool at room temperature. Unit weight, ultrasonic pulse, bending and compressive tests were carried out on these specimens. The effect of high temperature on the specimens was determined by calculating the unit weights, ultrasonic pulse velocity, bending and compressive strengths. Compressive and bending tests were tested in compliance with TS EN 196-1 standard (2016) and ultrasonic pulse velocity in compliance with TS EN 12504-4 standard (2012). At least 3 specimens were used for each test. The bending test was carried out in accordance with TS EN 196-1 (2016), using a single (middle) point loading method. In the bending test, the 4x4x16cm sized specimen was loaded at a speed of 50N/mm^2. At the end of the experiment, the maximum bending load that the specimen can carry was determined. In the compression test, specimens that were divided into two parts as a result of the bending test were used and loaded from their smooth side surfaces. Ultrasonic pulse velocity is determined ac-

cording to TS EN 12504-4 standard (2012). The experiment is based on determining the transition times of the ultrasonic pulse generated between the receiver and the transmitter within the specimens. For the unit weight test, each of the 4x4x16 cm sized specimens was weighed in the air-dry state. The specimen volume was calculated in cm3 using the dimension measurements made in the specimens according to TS EN 12390-1 (2013). The unit weight was calculated by dividing the specimen weight by the volume. Fig. 4 shows the cross sections of woodcrete specimens with different chip-cement ratios.

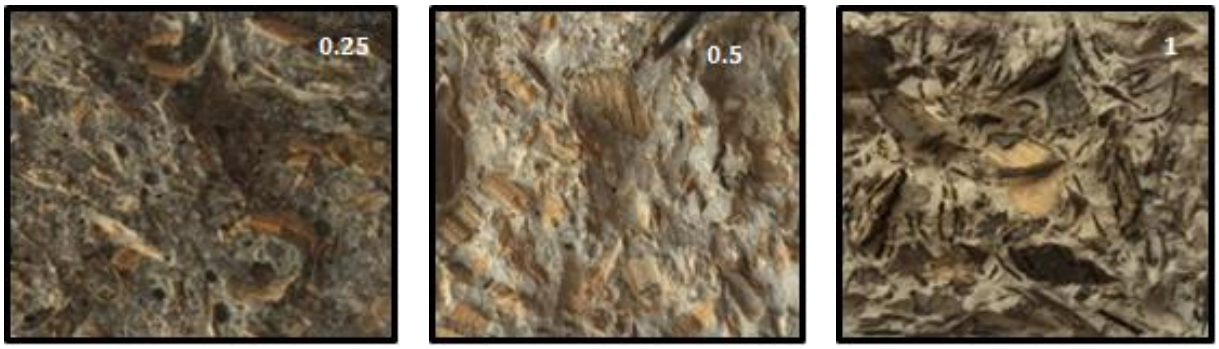

Fig. 4. Woodcrete sections.

3. Discussion

Unit weight, ultrasonic pulse velocity, bending and compressive strength values determined as a result of the experiments on control specimens are given in Table 4. When Table 4 is examined, as the chip-cement ratio increased, unit weight values decreased at rates reaching 12%, ultrasonic pulse velocity values reached 21% and compressive strength values reached 8.4% while bending strength increased by reaching 8.2%. The decrease in the amount of cement, which has a higher density compared to other components, caused a decrease in unit weights. Increasing the rate of chips, that transmit ultrasonic pulses more difficultly, decreased the ultrasonic pulse velocity. The increase in the number of chips, which have a weaker structure than cement, reduced their compressive strength. As a result of the fibrous structure of the chip, the bridging effect on the internal structure caused an increase in the bending strength. According to the strength results obtained, it has been seen that these composites can be used in masonry structures and in reinforced concrete structures as partition wall element. It has been determined that their strength is higher than alternative building materials such as brick and aerated concrete block.

Table 4. Test result of control specimens.

Chip-cement ratio	Ultrasonic pulse velocity, km/sec	Bending strength, MPa	Compressive strength, MPa	Unit weight, kg/dm^3
0.25	3.09	1.85	20.59	2.034
0.5	2.68	1.91	20.03	1.951
1	2.45	2.01	18.86	1.794

The change of unit weights of woodcrete specimens produced with different chip-binder ratios with high temperature is given in Fig. 5. When Fig. 5 is analysed, with increasing chip-cement ratio, cement density is higher than chip. Therefore, it was observed that the unit weights of the specimens decreased. It was observed that unit weights decreased regardless of the chip-cement ratio with increasing temperature. Since the temperature reached 200°C, decreases were observed in unit weights. These values decreased by 1.7% when using 0.25 chip-cement, 1.5% in 0.5 chip-cement, and unit weights decreased by 0.8% when using 1 chip-cement. The reason for this decrease can be explained by the evaporation of the water in the open gaps in the specimens and the decrease in the weight of the material. Since the temperature reached 400°C, unit weights decreased by 16.3% in case of 0.25 chip-cement, 17.5% in case of 0.5 chip-cement, and 13.2% in case of chip-cement ratio of 1. At 400°C, $Ca(OH)_2$, occurred at the end of the hydration reaction of cement, loses the water in its structure and turns into CaO, internal pressure caused by the evaporation of the gel waters trapped in the closed pores created micro cracks in the specimens, and these cracks and deteriorations caused a significant decrease in unit weights.

The change of the ultrasonic pulse velocity of the specimens with the temperature increase is given in Fig. 6. When Fig. 6 is examined, the decrease in the chip rate of the specimens increased the ultrasonic pulse velocity. According to a rigid structure such as cement paste, the low ultrasonic pulse velocity caused this decrease. It was observed that ultrasonic pulse velocity decreased in all specimens with increasing temperature. At 200°C, this decrease rate was 10.8% in the case of using 0.25 chip-cement ratio,

10.4% in the case of 0.5 chip-cement ratio, and 5.2% in the case of 1 chip-cement ratio. At 400°C, the reduction rates were determined as 85.7% in the use of 0.25 chip-cement ratio, 82.6% in the use of chip-cement ratio at 0.5, and 81.2% in the use of chip-cement ratio at 1. The gaps and micro cracks caused by the loss of water at 200°C in the specimens caused a slight decrease in ultrasonic pulse velocity. However, the reason for the considerable decrease in the ultrasonic pulse velocity at 400°C can be explained as the chemical degradation with the increase of cracks in addition to the loss of water and the carbonization of the chip by being affected by the high temperature.

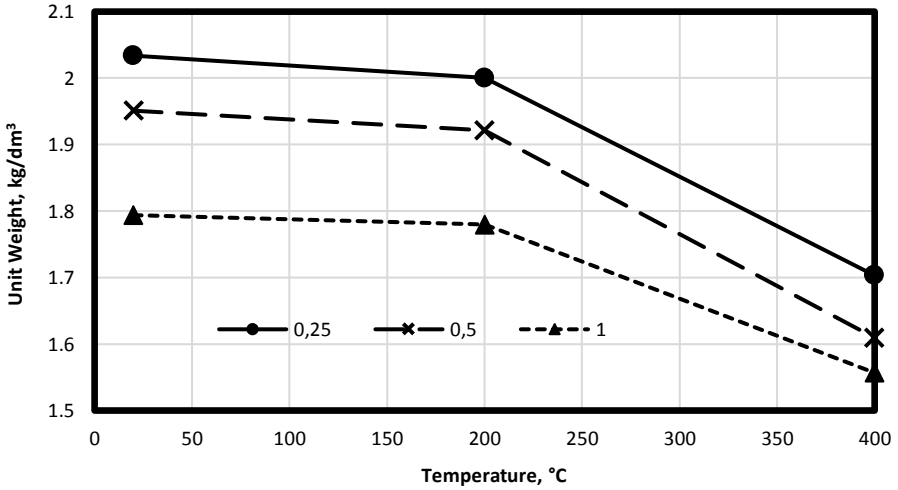

Fig. 5. The effect of high temperature on unit weights of woodcrete specimens.

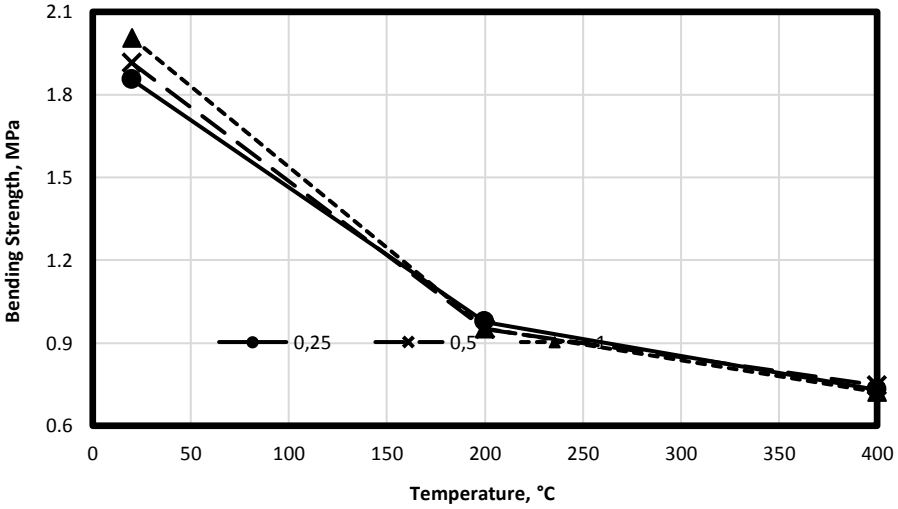

Fig. 6. Effect of high temperature on bending strength of woodcrete specimens.

The bending test results of the specimens are given in Fig. 7. When the bending test results were examined, the increase in the amount of chip due to the fact that the chip behaved like fiber had a positive effect on the bending strength. It was observed that the bending strength values decreased with the increase in temperature under the influence of high temperature. This decrease was 47.4% in the case of using 0.25 chip-cement, 50.3% in the case of using 0.5 chip-cement, and 52.6% in the case of 1 chip-cement at 200°C. At 400°C, there was a 60.6% loss of strength in the use of 0.25 chip-cement, 61% in the use of chip-cement at 0.5, and 64% in the use of chip-cement at a rate of 1. In addition to being effective in the decrease in bending strength of water loss and chemical degradation in the binding phase due to its high temperature, the main effect is thought to be partially carbonized and losing its elasticity by the chips acting as fiber.

The compressive strengths remaining under the high temperature effect of the specimens are shown in Fig. 8. When Fig. 8 is examined, since the binding phase is more rigid than the chip, the increase in chip rate decreased the compressive strength. The increase in temperature negatively affected the compressive strength. The decrease in compressive strength was at 200°C, 4.8% in case 0.25 chip-cement, 12.9% in case 0.5 chip-cement, 49.3% in case 1 chip-cement; 400°C, 46.6% in case 0.25 chip-cement, approximately 50% in case 0.5 and 1 chip-cement found to be. The reason for this decrease can be said as the deterioration of CSH structure, which provides resistance in the binding phase, dehydration of

$Ca(OH)_2$, micro cracks caused by water loss, and the fibrous structure of the chip deteriorate due to the temperature and the chip acts as a gap. Despite these large decreases in the compressive strength of the specimens, the residual strengths are sufficient for masonry structures and non-bearing partition walls elements.

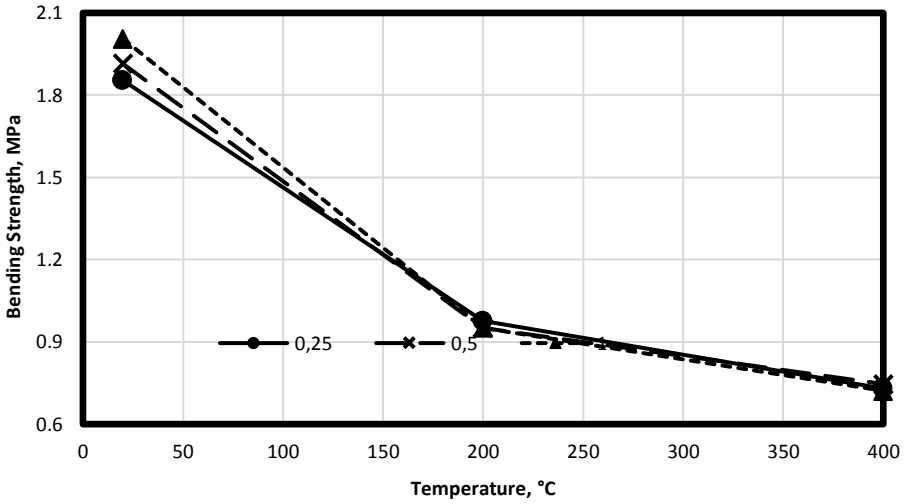

Fig. 7. Effect of high temperature on bending strength of woodcrete specimens.

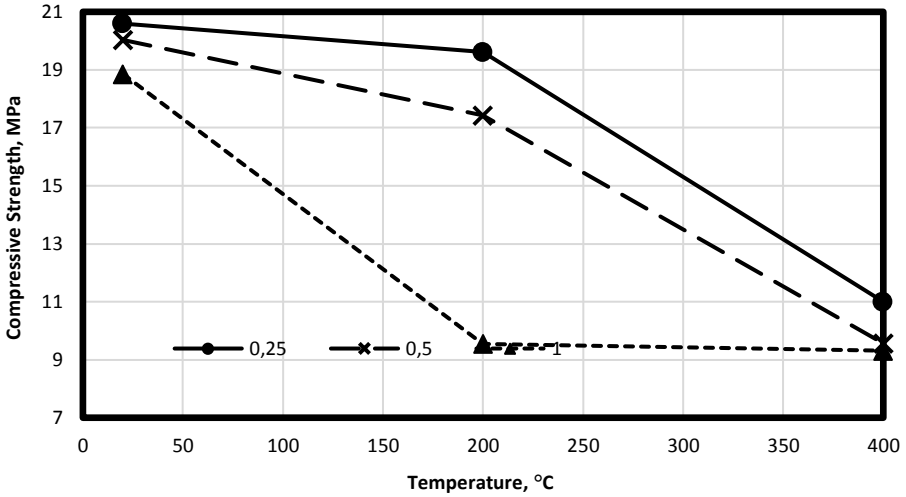

Fig. 8. Compressive strength variation of woodcrete specimens with high temperature.

4. Conclusions

As a result of the experiments conducted in this study, where the effect of high temperature on woodcrete properties was examined, the following results were obtained:

- Increasing the amount of chip decreased unit weight, ultrasonic pulse velocity and compressive strength while increasing bending strength.
- As the temperature increased, the unit weight values, which were 1.9 kg/dm^3 on average, decreased to 1.6 kg/dm^3 depending on the chip rate.
- While the highest losses are observed at ultrasonic pulse velocity with high temperature increase, the ultrasonic pulse velocity that remained as a result of these losses decreased to 0.5 km/sec.
- Despite the positive effect of chip content on bending strength, high temperature effect has been negatively affected by bending strengths and bending strength has decreased to 0.7 MPa.
- Even though there is a decrease in compressive strength with the increase of temperature, it is an important result that the remaining strengths are at an average level of 10 MPa and that this material does not completely lose its bearing strength under the influence of temperature.

As a result of this study, it can be suggested to use the chip waste generated during wood processing in cement-based composites at the ratio of 0.5 chip-cement. However, considering the losses caused by the high-temperature effect, it can be suggested to choose a chip-cement ratio of 0.25 if these products are used in places where they may be affected by high temperatures. In addition, the determination of other physical and chemical durability properties is recommended for other studies.

REFERENCES

Aigbomian EP, Fan M (2013). Development of wood-crete from hardwood and softwood sawdust. *The Open Construction and Building Technology Journal*, 7, 108-117.

Aras U, Kalaycıoğlu H, Yel H, Çok A (2019). Effect of cement and accelerator types on the physico-mechanical properties of cement-bonded particleboards. *Journal of Anatolian Environmental and Animal Sciences*, 4(4), 627-630.

Aras U, Kalaycıoğlu H (2016). Wood based composites and application areas. *International Refereed Journal of Engineering and Sciences*, 6(3), 120-136.

Ateş E (2018). Determination of the amount of the waste wood dust and its energy value in the city center of Balıkesir. *Technological Applied Sciences*, 13(4), 329-346.

Bozkurt Y (1982). Cemented particleboards. *Journal of Istanbul University Faculty of Forestry*, 32(2), 30-34.

DelaGree GD, Yu QL, Brouwers HJH (2014). Wood-wool cement board: optimized inorganic coating. *Proceedings of the 14th International Inorganic-Bonded Fiber Composites Conference* (IIBCC), 15-19, Da Nang, Vietnam.

EN 633 (1993). Cement-Bonded Particleboards- Definition and Classification. European Standard, Turkey.

İstek A, Gençer A (2014). The effect of pumice usage on cemented chipboard properties. *II. National Mediterranean Forest and Environment Symposium*, 550-567, Isparta, Turkey.

Jorge FC, Pereira C, Ferreira JM (2004). Wood-cement composites: A review. *Holz als Roh- und Werkstoff*, 62(5), 370-377.

Kalaycıoğlu H, Yel H, Çavdar AD (2012). Cemented wood wool composites and their usage areas. *Kastamonu University Faculty of Forestry Journal*, 12(1), 122-133.

Kaya Aİ (2020). Some wood based composite materials. *Turkchem News Portal*, Turkey.

Mengeloğlu F, Alma MH (2002). Using wheat stems in composite plate production. *Kahramanmaraş Sütçü İmam University Journal of Science and Engineering*, 5(2), 37-48.

Miller DP, Moslemi AA (2007). Wood-cement composites: effect of model compounds on hydration characteristics and tensile strength. *Wood and Fiber Science,* 23(4), 472-482.

Na B, Wang Z, Wang H, Lu X (2014). Wood-cement compatibility review. *Wood Research*, 59(5), 813-826.

Onursal FR (1996). Investigation of physical and mechanical properties of wood sawdust cement composite. *Graduate School of Science Thesis*, Istanbul Technical University, İstanbul, Turkey.

Risbrudt CD, Ritter DMA, Wegner TH (2010). Centennial edition wood handbook wood as an engineering material. University of Wisconsin, Forest Products Laboratory, *General Technical Report* FPL-GTR-190. Madison, WI: U.S. 508 p.

Simatupang MH, Geimer RL (1990). Inorganic binder for wood composites: feasibility and limitations. *Proceedings of Wood Adhesive Symposium, Forest Product Resources Society*, 169-176, Madison, Wisconsin, USA.

Şahin HT (2019). Cement binder wood composites: general features. *Turkchem News Portal*, Turkey.

Şahin HT, Kaya Aİ, Yalçın ÖÜ, Kılınçarslan Ş, Şimşek Y, Mantanis GI (2019). Study on the production process and properties of cement-based wood composite materials. *The Journal of Graduate School of Natural and Applied Sciences of Mehmet Akif Ersoy University*, 10(2), 219-228.

TS EN 196-1 (2016). Methods of testing cement - Part 1: Determination of strength. Turkish Standardization Institute, Ankara, Turkey.

TS EN 1363-1 (2013). Fire resistance- Tests- Part 1: General requirements. Turkish Standardization Institute, Ankara, Turkey.

TS EN 12390-1 (2013). Testing hardened concrete - Part 1: Shape, dimensions and other requirements for specimens and moulds. Turkish Standardization Institute, Ankara, Turkey.

TS EN 12504-4 (2012). Testing concrete - Part 4: Determination of ultrasonic pulse velocity. Turkish Standardization Institute, Ankara, Turkey.

Ulusoy H, Peker H (2019). Composite production and use in wood industry. *3rd International Symposium on Innovative Approaches in Scientific Studies*. 4(1), 595-598.

Wang L (2018). Value-added recycling of construction waste wood into eco-friendly cement-bonded particleboards. *Ph.D thesis*, The Hong Kong Polytechnic University, Hong Kong.

Wei YM, Tomita B (2001). Effects of five additive materials on mechanical and dimensional properties of wood cement-bonded boards. *Journal of Wood Science,* 47(6), 437-444.

Wolfe RW, Gjinolli A (1996). Cement-bonded wood composites as an engineering material. *The Use of Recycled Wood and Paper in Building Applications*, 84-91.

Challenge Journal of Concrete Research Letters

Research Article

Fracture properties of self-compacting fiber-reinforced concrete

Mariam Farouk Ghazy [a,*], Metwally Abd Allah Abd Elaty [a], Omar Daboun [b]

[a] *Department of Structural Engineering, Tanta University, PC 31733 Tanta, Egypt*

[b] *Department of Civil Engineering, Delta Higher Institute for Engineering and Technology, Mansoura, Egypt*

ABSTRACT

Self-compacting concrete (SCC) is an innovative concrete that does not necessitate vibration for placing and compaction. Nineteen concrete mixes were investigated including a control mix without fibers as well as eighteen SCC with fibers (SCFRC) mixes. Three types of fibers (polypropylene, glass and steel) were used. Slump flow, L-box, V-funnel as well as column segregation tests were conducted to assess the fresh properties. Whereas, compressive, splitting tensile and flexural strengths were measured to assess the hardened properties of SCFRC. Three point bending tests were performed for the purpose of assessing the fracture properties of SCFRC. Test results showed that the inclusion of fibers to produce SCFRC mixtures remarkably enhanced the fracture properties including fracture energy (G_f) and fracture toughness (K_{1c}). Inclusion of steel fibers with 2% volume fractions showed an improvement with 26.9 times for G_f over the control mix. Whereas, 104% increase in K_{1c} was recorded for the same mix over the mix without fibers. Adding fibers to SCC to produce self-compacting fiber reinforced concrete (SCFRC) will expand its advantages. However, the application fields still need to understand the properties of SCFRC.

ARTICLE INFO

Article history:
Received 10 July 2020
Revised 11 October 2020
Accepted 19 November 2020

Keywords:
Self-compacting concrete
Fiber-reinforced concrete
Fresh properties
Fracture properties

1. Introduction

The Japanese researchers and engineers took the responsibility of developing a special kind of concrete that can be placed and finished with less skilled laborers. Consequently, the notion of Self-compacting concrete (SCC) was first generated in Japan in 1986 (Douglas, 2004). SCC is an innovative concrete that does not necessitate vibration for placing and compaction. It is fully filling formwork and attaining full compaction under its own weight without the requirement, of any type of compacting or external vibration. High segregation resistance, great passing ability and exceptional ability to flow around obstacles, congested steel reinforcement and tight sections are the three main advantages of SCC (Okamura and Ozawa, 1995). SCC also has another major benefit compared to traditional concrete, it is used to minimize the noise level in construction sites and decrease the impact on the environment (Persson, 2001). In addition to accelerate the rate of concrete casting, diminishing construction times, improving the quality of concrete and reducing the overall cost are also benefit of its implementation.

Adding fibers to SCC to produce self-compacting fiber-reinforced concrete (SCFRC) will expand its advantages. Fibers bridge cracks and restrict its ingeneration and therefore enhance flexural and tensile strengths (Groth and Nemegeer, 1999; Khayat and Roussel, 1999; Alberti et al., 2014a; Ghazy et al., 2015; Hoang and Fehling, 2017; Adhikary et al., 2019).

Fracture mechanics is the field of solid mechanics involved in the study of the expansion of cracks in materials and the quantitative relations between the crack length, the material's deep-rooted resistance to crack growth, and the stress at which the crack expands at high speed to cause structural failure. The crack path through a composite material such as concrete is dependent on the mechanical interaction between the aggregates and the binder matrix. Fracture energy (G_f) of a composite material which is defined as the amount of energy necessary to create one-unit area of a crack (Barros and Figueiras, 1999). The result of G_f depends on the deviation of the

* *Corresponding author*. Tel.: +2-040-345-0532 ; Fax: +2-040-345-3860 ; E-mail address: mariam.ghazy@f-eng.tanta.edu.eg (M. F. Ghazy)
ISSN: 2548-0928 / DOI: https://doi.org/10.20528/cjcrl.2020.04.004

crack path from an idealized crack plane (Sabir et al., 1997; Wittmann, 2002). The value of fracture toughness (K_{1c}) indicates the magnitude of the stress concentration in front of the crack tip when the crack starts to propagate.

Tension stiffening is the ability of concrete to carry tension between cracks, which provides additional stiffness for a RC member in tension before the reinforcement yields. It can significantly affect member rigidity, deflection, and width of cracks under service loads. The presence of steel fibers is effective in controlling splitting cracks and significantly increases the tension stiffening effect because SFRC can carry tensile stress through the crack (Morelli et al., 2017; Kytinou et al., 2020).

Adding steel or/and polypropylene fibers ranging from 0.25% to 1% showed that fiber bridges cracked on the fracture surface during the loading and delayed cracking, thus the element did not break as well as an extended post-peak softening behavior did occur. The shape of the descending branch was dependent on geometrical properties, mechanical properties and the quantity of the used fibers (Ghazy et al., 2015; Smarzewski and Barnat-Hunek, 2015).

Addition of low, medium and high fiber contents of macro polyolefin fibers to SCC was showed that the G_f obtained for all the polyolefin SCFRC mixtures is significantly higher when compared with the plain SCC. K_{1c} and ductility improvements are quite reliable even for the medium polyolefin fiber content mixtures based on Alberti et al. (2014b).

Biswajit and Mohanty (2015) added steel fibers to SCC then investigated the fracture properties of the produced SCFRC. The relationships between load and crack mouth opening displacement (CMOD) diagrams for SCFRC showed an increase in fracture energy properties of the SCFRC mixes owing to crack arresting mechanism of the fibers in the matrix. They concluded that the mixes including 0.2% and 0.25% steel fiber by weight of concrete exhibited best performance.

An experimental study to investigate fracture behavior of hybrid steel SCFRC was performed by Akcay and Tasdemir (2012). Three different types of steel fibers with and/or without hooked-ends were added to the mixtures in two different volume fractions (0.75% and 1.5% of the total volume of concrete). Based on their G_f test results, the mixes with high strength steel fibers exhibited behavior of enhanced toughness and ductility when compared to the concretes with normal strength steel fibers.

Different ratios of the notch depth to beam depth were used in fracture test specimens, Elices and Planas (1996) conducted an analysis of test results for different notch to beam's depth ratios and showed that a ratio of 0.2–0.5 can be considered as a practical experimental range. A ratio of 0.375 was used in the specimens of that study to make the ligament area sizable in order to enable the observation of the crack propagation in the concrete. Three or four-point bending tests on notched beams were usually carried out to evaluate the material fracture energy. The three-point bending tests on center-notched beams are more suitable to characterize the fracture parameters of SFRC (Hordijk, 1991).

From the above previous studies, the application fields still need to understand the properties of SCFRC. The main target of this study is to determine the fracture parameters of SCFRC after inclusion of different types and volume fractions of fiber and to make comparisons with SCC without fibers. For this purpose, load–deflection curves, G_f, K_{1c} and CMOD were calculated and assessed to investigate the fracture properties from three point bending tests on SCFRC notched beams.

2. Experimental Program

2.1. Materials

Natural siliceous sand with a specific gravity of 2.55 and a fineness modulus of 2.46 was used. The coarse aggregate used was crushed dolomite, with a specific gravity of 2.6. The crushing modulus was 23%, and the maximum nominal size was 10 mm.

The cement used was Portland cement (CEM I 42.5N) according to (ESS 4756-1-13), and (EN 197-1-11). Tap water free from impurities was used for mixing and curing the test specimens. Silica fume (SF) with specific gravity of 2.21 and specific surface area of 150000 cm^2/g was used and Class (F) fly ash (FA) meeting the requirements of ASTM C618-19 with a specific gravity of 2.1 was used.

High range water reducer admixture (HRWR) was used. The admixture is a brown liquid having density of approximately 1.080 kg/L at room temperature. The admixture permissible percentage is 1-3% of cement weight according to the manufacturer which is the polycarboxylic ether based and meeting the standard requirements of ASTM C494/C494M-19 (type F and G).

Three types of fibers, mainly, polypropylene (PP), glass (G) and steel (S) (straight fibers) were used. For PP fibers, two different shapes were used including straight and mesh. Moreover, two different aspect ratios of PP were conducted. The properties of the investigated fibers according to the manufacturer are presented in Table 1.

Table 1. Properties of the investigated fibers.

Type / shape		Length (L) (mm)	Diameter (d) (mm)	L/d	Modulus of elasticity (GPa)	Tensile strength (MPa)
Polypropylene fibers (PP)	Micro straight fibers (PM)	6	0.018	333	9	500
	Long straight fibers (PL)	18	0.018	1000		
	Micro fiber mesh (PF)	6	0.018	333		
	Long fiber mesh (PFL)	18	0.018	1000		
Glass fibers (G)		18	0.018	1000	72	1700
Steel fibers (straight) (S)		15	1	15	210	1250

2.2. Mix proportional

Nineteen concrete mixes were investigated including a control SCC mix without fibers as well as eighteen SCFRC mixes. The used fiber volume fractions were 0.25%, 0.5% and 0.75% by volume of concrete for the conducted PP fibers. Whereas, 0.15%, 0.25% and 0.4% volume fraction for G fibers were investigated. On the other hand, 0.5%, 1.0% and 2.0% volume fraction for S fibers were included. The net water to cementitious materials ratio (w/cm) for this study was varying from 27% to 39% and HRWR dosage used ranged from 1.5% to 2% (by weight of total cementitious materials) depending on fiber type and volume fraction. Concretes were produced by using SF and FA with percentages of 10% and 20% by weight of total cementitious materials, respectively. The concrete mix proportions for all mixes are detailed in Table 2.

Table 2. Concrete mix proportions, kg/m^3.

Fiber Type	Mix ID	F%	w/cm	C	FA	SF	Dolomite	Sand	Water	HRWR
Without fibers	SCC-0	0	0.27	420	120	60	700	700	162	9
Polypropylene micro fibers (PM), 6 mm	SCC-PM0.25	0.25	0.29	420	120	60	700	700	174	9
	SCC-PM0.5	0.5	0.31	420	120	60	700	700	186	12
	SCC-PM0.75	0.75	0.32	420	120	60	700	700	192	12
Polypropylene Long fibers (PL), 18 mm	SCC-PL0.25	0.25	0.29	420	120	60	700	700	174	9
	SCC-PL0.5	0.5	0.3	420	120	60	700	700	180	10.5
	SCC-PL0.75	0.75	0.38	420	120	60	700	700	228	12
Polypropylene micro fiber mesh (PF), 6 mm	SCC-PF0.25	0.25	0.29	420	120	60	700	700	174	9
	SCC-PF0.5	0.5	0.29	420	120	60	700	700	174	9
	SCC-PF0.75	0.75	0.3	420	120	60	700	700	180	10.5
Polypropylene long fiber mesh (PFL), 18 mm	SCC-PFL0.25	0.25	0.29	420	120	60	700	700	174	9
	SCC-PFL0.5	0.5	0.29	420	120	60	700	700	174	9
	SCC-PFL0.75	0.75	0.31	420	120	60	700	700	186	12
Glass fibers (G), 18 mm	SCC-G0.15	0.15	0.31	420	120	60	700	700	186	10.5
	SCC-G0.25	0.25	0.36	420	120	60	700	700	210	12
	SCC-G0.4	0.4	0.39	420	120	60	700	700	234	12
Steel fibers (S), 15 mm	SCC-S0.5	0.5	0.29	420	120	60	700	700	174	9
	SCC-S1	1	0.29	420	120	60	700	700	174	9
	SCC-S2	2	0.29	420	120	60	700	700	174	9

Note: F: Fibers, C: Cement, FA: Fly ash, SF: Silica fume

2.3. Specimen preparation

The dry materials required for each mix were weighted and mixed using a drum concrete mixer with 100 L total capacity. The water in addition to admixture and cementitious materials were mixed for a half minute to ensure the uniformity of the constituents. Sand was simultaneously charged into the mixer and was mixed for a half minute and then coarse aggregate was added and continue mixing for at least two minutes, finally fiber was added and then the mix was mixed for another 5 minutes.

The conducted specimens in this study for fracture test were 100 mm breadth (b), 80 mm depth (d) and 250 mm long (L) with a 30 mm notch (a) in the middle of the beam. Cubes with 100 mm side length were used for determining compressive strength. Whereas, cylinders with 100 mm diameter and 200 mm length were used for determining splitting tensile strength. On the other hand, prism specimens with a square section of the 100 mm side length and 500 mm total length were used to determine the flexural strength.

The concrete was placed in the steel molds without any compacting or vibrating, finally surfaces were finished using towel. All of the specimens were kept in their molds for 24 h after casting in moisture room at 25°C and 50% relative humidity, then they were removed from the molds and remarked with ID's then immerged in clean water at 20°C until the day of testing. All of specimens which tested after 56 days were taken out from the water after 28 days and kept in moisture room at 25°C and 50% relative humidity.

2.4. Testing procedures

Slump flow, L-box, V-funnel according to EFNARC-05 and Egyptian Technical Specification for Self Compacting Concrete (ESS 360-08) as well as column segregation tests according to ASTM C1610-19 were used to evaluate the consistency and workability of the fresh mixes of SCFRC. The slump flow test characterizes the flowability of the SCC, the V-funnel gives an indication of the viscosity and the increase of resistance to flow caused by the fibers, the L-box with reinforcement bars gives an indication of

passing ability through reinforcement, while the column segregation test evaluates stability of SCC against segregation. On the other hand, compressive strength, splitting tensile strength as well as flexural strength, were measured to assess the hardened properties of SCFRC.

Three point bending tests were performed by Universal Testing Machine (300 kN) for the purpose of assess the fracture properties of SCFRC. The ends of the specimens were placed on the supporting rollers at a span of 200 mm with the notch on tension side. Depth to notch ratio of 0.375 was used in the specimens of this study in line with Elices and Planas (1996) in order to enable the observation of the crack propagation in the concrete. Digital data acquisition system was incorporated with a load cell to record the load with an accuracy of 0.001 kN. The vertical displacement was measured by LVDT with an accuracy of 0.001 mm and 30 mm total capacity. The CMOD was measured by using Pie-shape (PI-5-100) fixed at the beam side. The Pie-shape was 100 mm gauge length, ± 5 mm capacity, 350Ω resistance and allowable bridge excitation of 10V. The data acquisition system had the ability to record up to 1000 data per second. A loading rate of 0.1 mm/min was used in the tests of this study. A high rate of data scanning per second was used to capture the post-peak part of the load–deflection curve. The load–deflection data were plotted to calculate the area under the curve.

The fracture energy (G_f) is the amount of energy necessary to create a crack on unit surface area projected in a plane parallel to the direction of propagation of crack, it is calculated from the work of fracture by using Eq. (1) according to RILEM TC 50–FMC.

$$G_f = \frac{W_0 + mg\delta_0}{A_{lig}} \quad (1)$$

where W_0 is the area under load deflection curve (N.m); mg is the self-weight of the specimen between supports (N), δ_{max} is the maximum displacement (m), A_{lig} is [b (d-a)] (m^2), b is the breadth of beam (m), d is the depth of beam (m), and a is the depth of notch.

K_{1c} is used to indicate the magnitude of the stress concentration that exists in front of the crack tip when the crack starts to propagate, Eq. (2) has been used in this study to calculate the K_{1c} (Bazant and Pfeiffer, 1987).

$$K_{1c} = \frac{3PL}{2bd^2} \times \sqrt{\pi a} \times \left[\frac{(1-2.5\,(A)+4.49(A^2)-3.98(A^3)+1.33(A^4)}{(1-A)^{3/2}}\right] \quad (2)$$

where P is the load (kN), A is a/d, L is the span of beam (m), b is the breadth of beam (m), d is the depth of beam (m), and a is the depth of notch (m).

3. Results and Discussion

3.1. Fresh concrete test results

The fresh properties test results of the investigated mixes are given in Table 3.

Table 3. Fresh properties test results.

Fiber Type	Mix ID	Slump flow		V-funnel		L-Box	Column Segregation
		D_{max}, mm	$t_{500\ mm}$, S	t_0, S	$t_{5\ min}$, S	H_2/H_1	S%
Without fibers	SCC-0	850	0.94	3.3	6.3	1	14.4
Polypropylene micro fibers (PM), 6 mm	SCC-PM 0.25	625	2	3.8	6.5	0.9	7.6
	SCC-PM 0.5	600	2.6	5	7	0.83	5
	SCC-PM 0.75	550	5	7	9.5	0.8	1
Polypropylene Long fibers (PL), 18 mm	SCC-PL 0.25	650	2.92	3.44	5.25	0.96	9.7
	SCC-PL 0.5	550	3	3.56	4.86	0.83	6.7
	SCC-PL 0.75	500	5.52	3.75	5.61	0.8	5.4
Polypropylene micro fiber mesh (PF), 6 mm	SCC-PF 0.25	750	1	3.41	4.87	0.96	5.6
	SCC-PF 0.5	625	1	3.91	5.26	0.93	4.5
	SCC-PF 0.75	600	1.26	4.68	5.89	0.88	2.5
Polypropylene long fiber mesh (PFL), 18 mm	SCC-PFL 0.25	650	2.5	4	6.48	0.96	9.1
	SCC-PFL 0.5	625	2.88	5.58	7.98	0.81	6.5
	SCC-PFL 0.75	580	4.85	6.79	8.15	0.8	5
Glass fibers (G), 18 mm	SCC-G 0.15	540	1.4	3.52	4.92	0.92	7.6
	SCC-G 0.25	500	2	4.8	6.1	0.85	5
	SCC-G 0.4	450	-	6.01	8.68	0.74	4.2
Steel fibers (S), 15 mm	SCC-S 0.5	850	1	3.73	3.91	1	9.4
	SCC-S 1	850	1.12	3.87	5.58	0.96	4.9
	SCC-S 2	800	1.15	4.22	6.19	0.93	1.4
Limits (EFNARC-05, and ESS 360-08)		600-800	2-5	6- 12	(t0+0) - (t0+3)	0.8-1	5-15 %

3.1.1. Slump flow test results

Slump flow test was carried out to ensure the horizontal free flow for the SCFRC. As seen in Table 3 the slump flow diameters D_{max} of all mixtures were in the range of 450-850 mm. Slump flow times $t_{500\ mm}$ were in the range of 0.94-5.52 S. The inclusion of fibers had a direct effect on the flow characteristics of SCC. The effect of different volume fractions and different aspect ratios of fiber on D_{max} is shown in Fig. 1.

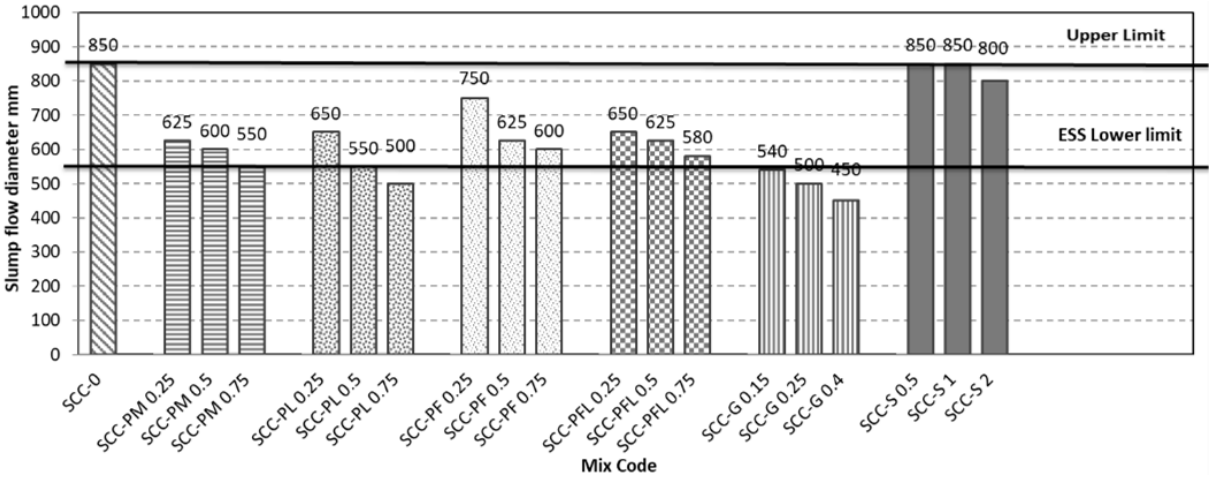

Fig. 1. Slump flow test results D_{max}.

3.1.2. L-Box test results

The L-box test is usually used to measure the filling and passing abilities. According to (EFNARC-05, and ESS 360-08) acceptance criteria for SCC, blocking ratio (H_2/H_1) should range from 0.8 to 1. The values of H_2/H_1 seem to be sensitive for G fibers addition. Whereas, H_2/H_1 seem to be less sensitive when PP and S fibers are added. Regardless of the fiber type, the increase in fiber volume fractions resulted in a drop in filling and passing abilities.

3.1.3. V-Funnel test results

The V-funnel test is usually used to assess the viscosity and filling ability of SCC. The test results are being the time periods taken for concrete to flow out of a V-shaped funnel just after filling the funnel and after 5 min (t_0, $t_{5\ min}$). The V-funnel test principal, apparatus, procedure and result computation are further described in (EFNARC-05, and ESS 360-07). Although increasing fiber volume fraction increased the t_0, but the difference between (t_0 - $t_{5\ min}$) ranged from 0.18 to 2.67 S that meets the requirements of (EFNARC-05, and ESS 360-08).

3.1.4. Column segregation test results

The column segregation test is usually used to evaluate the stability of SCC against segregation. The column segregation test principal, apparatus, procedure and result computation are further described in (ASTM C 1610-19). The test results are being the segregation percentage calculated from Eq. (3). SCC is generally considered to be acceptable if the percentage of segregation is less than 15% (ASTM C 1610-19).

$$S\% = 2\left[\frac{(Ct-Cb)}{(Ct+Cb)}\right]x100 \quad (3)$$

where: $S\%$ is the static segregation in percent, Ct is the mass of coarse aggregate in the top section of the column, and Cb is the mass of coarse aggregate in the bottom section of the column.

The column segregation test results proved that adding fibers to SCC mixes to produce SCFRC mixes enhanced stability of SCC against segregation that was observed based on column segregation test results. This could be attributed to the restriction of fibers to settlement of coarse aggregate particles. The reduction in segregation is up to 93% for mix with Polypropylene micro fibers in compared to control mix without fibers.

3.2. Hardened properties test results

The compressive strength, splitting strength as well as flexural strength test results at 7, 28 and 56-day age for the conducted mixes as a function of fiber types and fiber volume fractions are presented in Table 4.

3.2.1. Compressive strength

The effect of different volume fractions and different aspect ratios of fibers on the compressive strength (f_{cu}) are presented in Fig. 2. The f_{cu} test results show a tendency to be reduced compared with the control mix. This may be due to the excess of water to cementitious materials ratios that were slightly increased to achieve the flow ability requirements. Moreover, this is agreed with that for traditional fiber-reinforced concrete for which the f_{cu} is not considered a target for improvement (Apeh and Ameh, 2020).

Table 4. Hardened properties test results.

Mix ID	Compressive strength (MPa)			Splitting tensile strength (MPa)			Flexural strength (MPa)			G_f (N/m)	K_{1c} (N/m$^{2/3}$)	CMOD (mm)
	7	28	56	7	28	56	7	28	56			
SCC-0	48.5	65.9	78	3.11	3.7	4.23	9.27	9.77	10.96	44.33	6.35	0.035
SCC-PM0.25	30	37.7	53.9	3.01	3.59	4.21	9.34	9.86	11.08	36.93	7.87	0.037
SCC-PM0.5	40.5	50	58.3	3.12	3.75	4.44	10.42	12.03	13.03	48.78	8.45	0.041
SCC-PM0.75	44.8	52.5	73	3.35	4.07	4.45	10.58	12.42	13.53	50.27	8.91	0.045
SCC-PL0.25	29.3	35	42	3	3.6	4.29	9.74	11.97	12.53	197.08	7.49	0.039
SCC-PL0.5	39.2	44.6	54.4	3.24	3.86	4.69	9.78	12.6	13.35	202.76	7.58	0.044
SCC-PL0.75	43.6	50.2	61	3.7	4.8	5.12	10.3	13.04	13.95	219	7.7	0.047
SCC-PF0.25	41	53.4	55.8	3.06	3.64	4.23	9.49	10.13	11.46	81	8.15	0.038
SCC-PF0.5	45	56	60	3.13	3.8	4.48	10.75	11.65	13.73	132.69	8.22	0.042
SCC-PF0.75	46.4	61	66.8	3.49	4.08	4.49	11.84	13.45	13.96	168.72	8.4	0.046
SCC-PFL0.25	39	54	61	3.13	3.71	4.74	9.62	11.43	11.93	120.87	5	0.045
SCC-PFL0.5	44.6	56.1	67.2	3.5	4.31	4.89	10.1	12.8	13.81	164.15	7.04	0.05
SCC-PFL0.75	48.3	62	71	3.9	4.96	5.36	10.43	13.77	14.2	175.07	10.43	0.065
SCC-G0.15	35.1	42.4	47	2.95	3.42	3.91	9.3	9.89	10.97	19.47	5.71	0.037
SCC-G0.25	42.9	50	57.5	3.12	3.82	4.1	9.68	9.99	11.3	21.45	7.12	0.04
SCC-G0.4	49	60	67.9	3.14	3.96	4.45	10.03	10.32	11.32	32.58	8	0.045
SCC-S0.5	40	49.6	66.3	4.21	4.79	5.53	11.1	12.1	14.23	346.33	8	0.051
SCC-S1	45	55	72.2	4.4	5.9	6.02	11.5	14.07	15.18	920.52	8.41	0.067
SCC-S2	55	64.5	84	5.58	6.83	6.97	12.1	14.94	15.95	1237.68	13	0.094

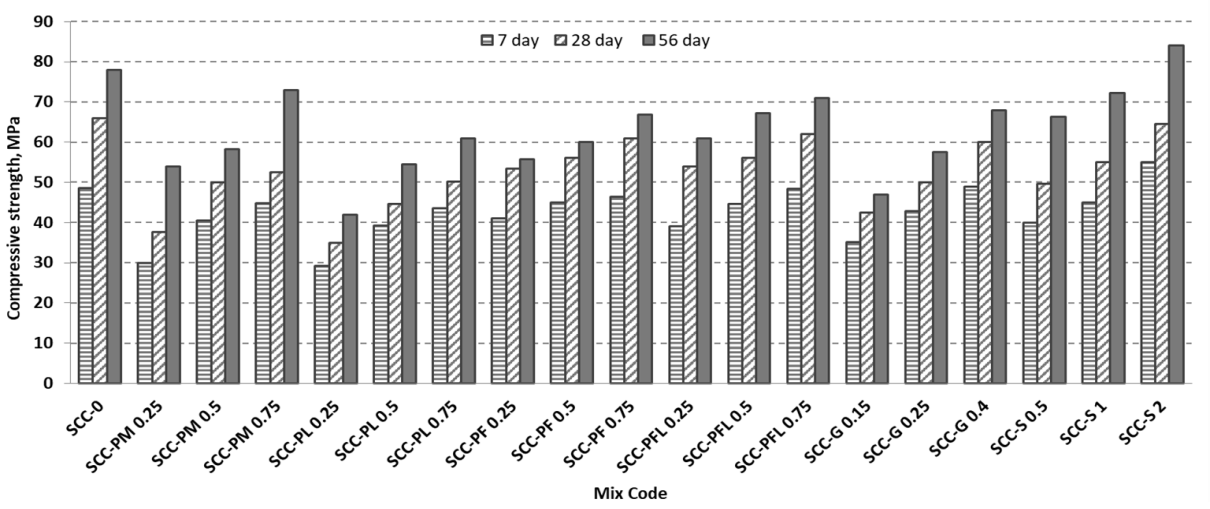

Fig. 2. Compressive strength test results.

3.2.2. Splitting tensile strength

The effect of different volume fractions and different aspect ratios of fibers on the splitting tensile strength (f_{sp}) are presented in Fig. 3. Mixes cast with the same type of fibers showed remarkable enhancements in the splitting tensile strength with ages. The maximum enhancements were 34%, 7% and 84.6%, for mixes incorporating PP, G and S fibers, respectively at 28-day compared to control mix SCC-0. The test results of f_{sp} indicated that the relativity higher efficiency of incorporating S fibers to enhance the f_{sp} compared with G and PP fibers.

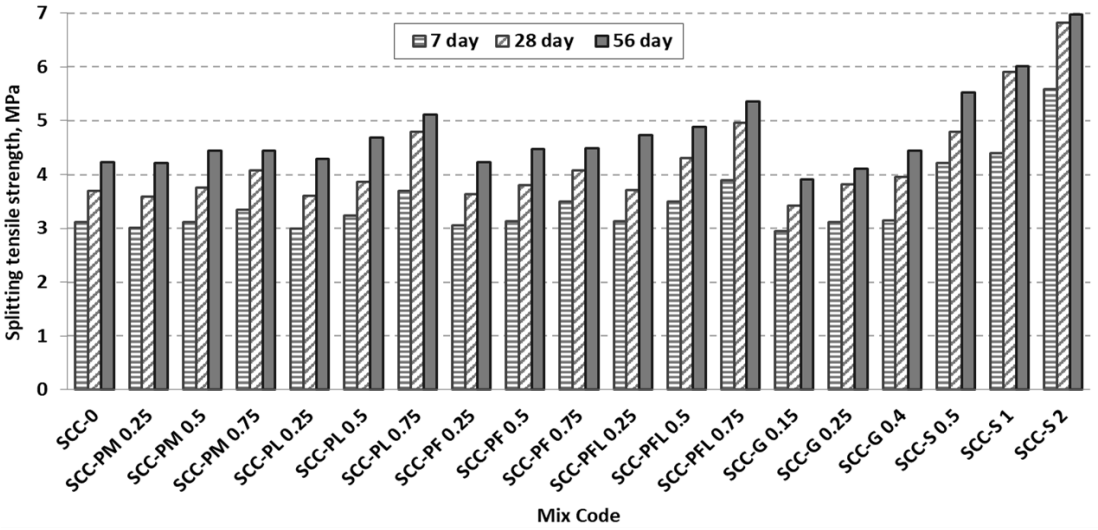

Fig. 3. Splitting tensile strength test results.

3.2.3. Flexural strength

The effect of different volume fractions and different aspect ratios of fiber on the flexural strength (f_f) are presented in Fig. 4. However, mixes cast with the same type of fibers showed remarkable enhancements in the f_f with ages. The maximum enhancements were 40.9%, 5.6% and 52.9% for mixes incorporating PP, G and S fibers, respectively at 28-day compared to control mix SCC-0.

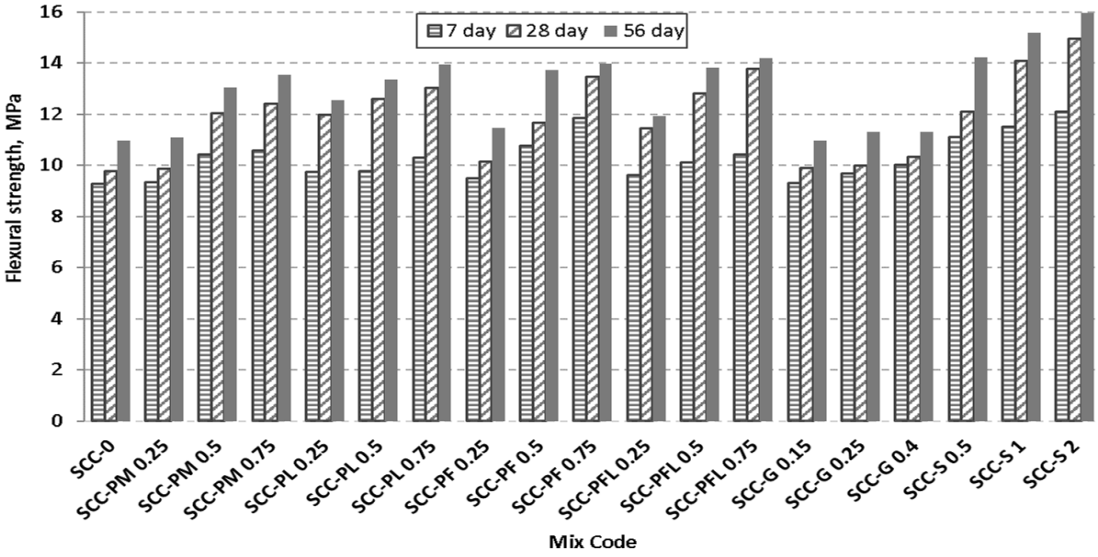

Fig. 4. Flexural strength test results.

3.3. Fracture properties test results

Fracture energy (G_f), fracture toughness (K_{1c}) and crack mouth opening displacement (CMOD) of the SCFRC were measured. The values of fracture properties are shown in Table 4.

3.3.1. Stress-deflection relationships

As the applied load on the notched beam increased, no cracks were observed until the load reached its peak value. A crack appeared at the end of the notch and started to propagate fast in the ligament when the load reached its peak value. The crack opened faster in the SCC specimens than in the SCFRC specimens. Failure occurred by opening of a single crack in the ligament in both types of concrete specimens. The stress deflection relationships of SCC and SCFRC specimens are given in Figs. 5 and 6. It is seen from these figures that the flexural stress increases with the increase of fiber volume fractions for all fiber types generally.

The post-peak parts of the stress–deflection curve "softening curves" seemed to be less steep with the increase of fiber volume fractions. The descending part of the stress–deflection curve, dropped faster in the SCC-0 specimen compared to that for the other SCFRC specimens.

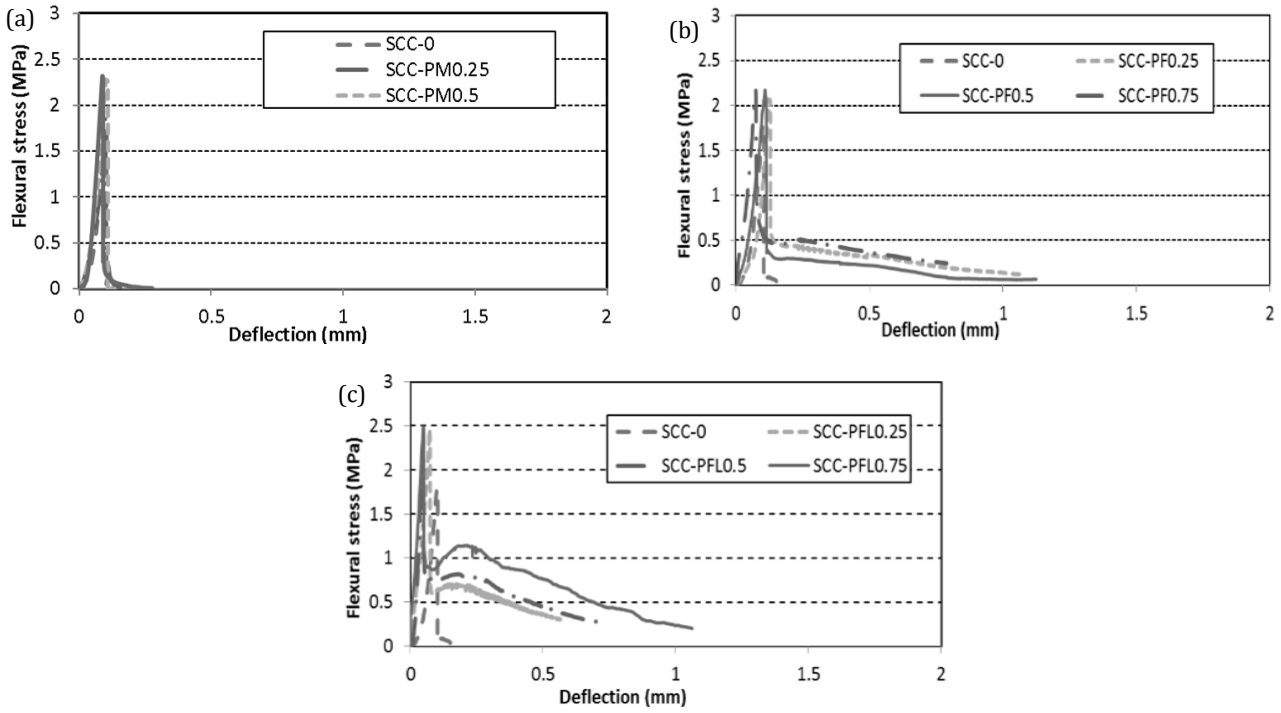

Fig. 5. Flexural stress vs deflection for notched specimens with polypropylene fibers: a) PP short fiber mesh; b) PP short fiber mesh; c) PP long fiber mesh.

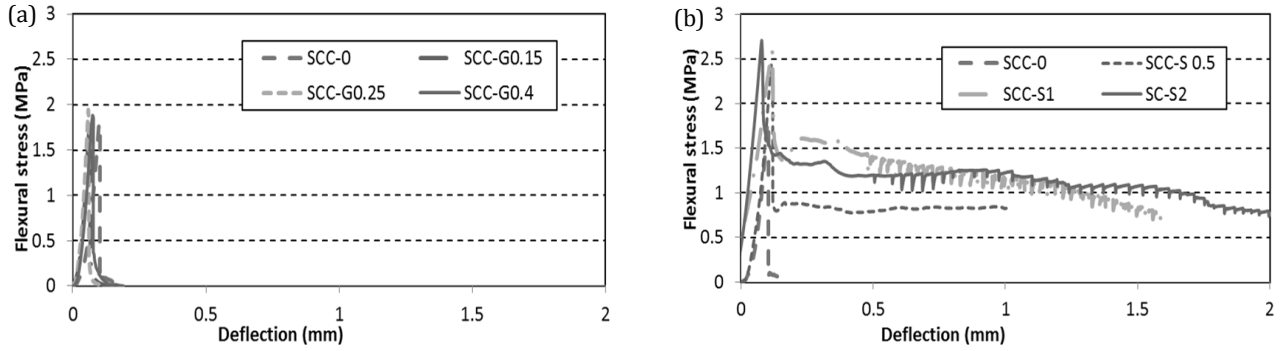

Fig. 6. Flexural stress vs deflection for notched specimens with fibers: a) Glass; b) Steel.

3.3.2. Effect of fiber types and volume fractions on fracture energy

The inclusion of fibers had a direct effect on the G_f of SCC. The effect of different types and volume fractions of fiber on G_f is plotted in Fig. 7. For mixes incorporating PP fibers, the G_f tends to increase with the volume fraction in all types of PP fibers. Increase the volume fraction of fiber from 0% to 0.75% increased the G_f, the maximum percentage increases were 13%, 394%, 279% and 295% for SCC-PM0.75, SCC-PL0.75, SCC-PF0.75 and SCC-PFL0.75, respectively compared to the control mix SCC-0. Whereas, the inclusion of G fibers did not improve the G_f of SCC but on the contrary had a slightly negative effect. This may be due to the relatively higher w/cm ratio used to maintain the SCC requirements. On the other hand, mixes containing S fibers showed a massive effect on the fracture energy of SCC, the. Increase the volume fraction of fiber from 0% to 2% increased the G_f. The maximum increases were 6.81, 19.67 and 26.92 times for SCC-S0.5, SCC-S1 and SCC-S2, respectively over the control mix SCC-0.

3.3.3. Effect of fiber type and volume fraction on fracture toughness

The effect of different types and volume fractions of fiber on the K_{1c} is plotted in Fig. 8. For mixes incorporating PP fibers, the K_{1c} tends to increase with the volume fraction, increases the volume fraction of fiber from 0% to 0.75% improved the K_{1c}, the maximum percentage enhancements were 40%, 21%, 32% and 64% for SCC-PM0.75, SCC-PL0.75, SCC-PF0.75 and SCC-PFL0.75, respectively compared to SCC-0. Whereas, the inclusion of G fibers slightly improves the K_{1c} of SCC, in case of SCC-G0.15 the percentage increase is not enough to reach the K_{1c} of SCC-0 and the increases were 12% and 25% for SCC-G0.25 and SCC-G 0.4, respectively, compared to SCC-0. On the other hand, for S fibers the maximum increases were 24%, 32% and 104% for SCC-S0.5, SCC-S1 and SCC-S2, respectively over to the control mix SCC-0.

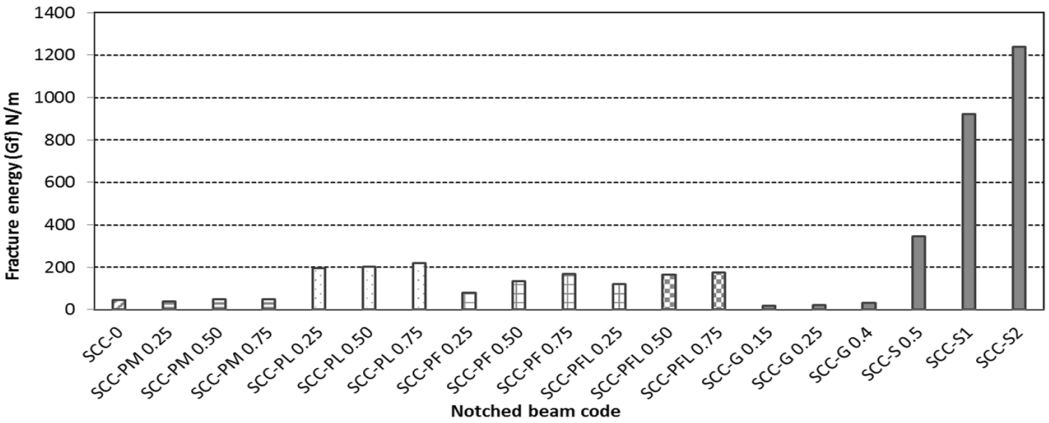

Fig. 7. Effect of fiber types and volume fractions on G_f.

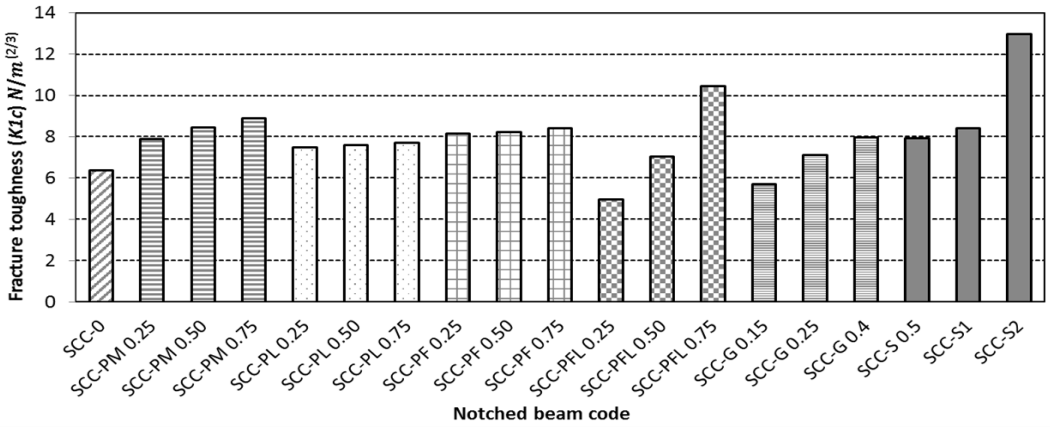

Fig. 8. Effect of fiber types and volume fractions on K_{1c}.

3.3.4. Effect of fiber types and volume fractions on crack mouth opening displacement

Results of CMOD for the investigated mixes are shown in Fig. 9. The CMOD is ranged from 0.035 mm to 0.067 mm. Regardless the fiber types, increasing the volume fraction of fibers increased the CMOD. For mixes containing PP fibers, the increases were 28.5%, 34.2%, 31.4% and 85.7% for SCC-PM0.75, SCC-PL0.75, SCC-PF0.75 and SCC-PFL0.75, respectively compared to SCC-0. Whereas, the increases for mixes incorporating G fibers were 5.7%, 14.2% and 28.5% for SCC-G0.15, SCC-G0.25 and SCC-G0.4, respectively compared to SCC-0. On the other hand, the increases for mixes incorporating S fibers were 45.7%, 91.4% and 168.5% for SCC-S0.5, SCC-S1 and SCC-S2, respectively compared to control mix SCC-0.

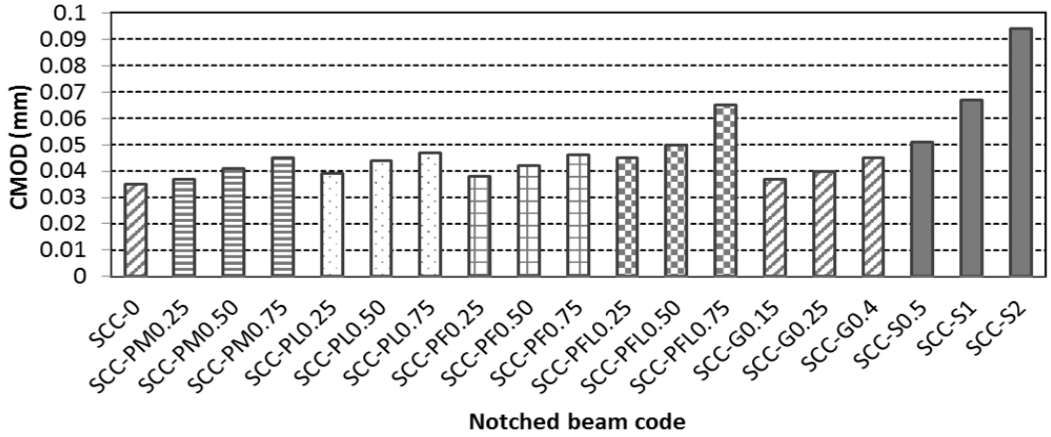

Fig. 9. Effect of fiber types and volume fractions on CMOD.

4. Conclusions

Based on the work performed in this study and the analysis conducted, the following conclusions could be drawn:

- Adding fibers to SCC mixes to produce SCFRC mixes enhanced stability of SCC against segregation that was observed based on column segregation test results. This could be attributed to the restriction of fibers to settlement of coarse aggregate particles. The reduction in column segregation test results was up to 93% with respect to control mix.
- In term of strength properties, concrete mixes incorporating steel fibers achieved higher compressive strength than polypropylene and glass fibers. The increase in compressive strength was up to 7.7% at 2% steel fibers compared to control mix without fibers at 56 days age. Whereas, the increases were remarkable in splitting tensile and flexural strengths, the increases were 84.6% and 52.9%, respectively at 28 days age.
- The efficiency of the conducted fibers in strength properties can be arranged in an ascending order at steel, polypropylene, and glass fibers, respectively.
- The inclusion of steel fibers had massive effect on the fracture energy of SCFRC. Using of 2% steel fibers enhanced G_f, by 26.9 times. Whereas, the maximum enhancement was 3.94 times over the control mix without fibers when 0.75% polypropylene fibers volume fraction was added.
- For the conducted fibers, using of 0.75% of polypropylene fibers enhanced the K_{1c} by 40%, 21%, 32% and 64% for mixes with polypropylene micro fibers, polypropylene Long fibers, polypropylene micro fiber mesh and polypropylene long fiber mesh, respectively. Whereas, only 25% enhancement was recorded when 0.4% glass fibers volume fraction was used. On the other hand, adding 2% steel fibers increased K_{1c} by 104%.
- Regardless of the fibers type, the increase in fiber volume fraction increased the CMOD. The increases were 28.5%, 34.2%, 31.4% and 85.7% for mixes with polypropylene micro fibers, polypropylene Long fibers, polypropylene micro fiber mesh and polypropylene long fiber mesh, respectively, when 0.75% polypropylene fibers volume fraction was added. Whereas, the increase was 28.5% when 0.4% glass fibers volume fraction was added. On the other hand, adding 2% steel fibers volume fraction increased CMOD by 168.5%.

Acknowledgements

The authors would like to express thanks are to staff of the Laboratory of Properties of Materials, Tanta University, Tanta, Egypt for their supports.

References

Adhikary SK, Rudzionis Z, Balakrishnan A, Jayakumar V (2019). Investigation on the mechanical properties and post-cracking behavior of polyolefin fiber reinforced concrete. *Fibers*, 7(1), 1–8.

Akcay B, Tasdemir M (2012). Mechanical behavior and fiber dispersion of hybrid steel fiber reinforced self-compacting concrete. *Construction and Building Materials*, 28, 287–293.

Alberti M, Enfedaque A, Gálvez J (2014a). On the mechanical properties and fracture behavior of polyolefin fiber-reinforced self-compacting concrete. *Construction and Building Materials*, 55, 274–288.

Alberti MG, Enfedaque A, Gálvez JC (2014b). On the mechanical properties and fracture behavior of polyolefin. *Construction and Building Materials*, 55, 274–288.

Apeh JA, Ameh JE (2020). Properties of steel fiber self-compacting concrete incorporating quarry dust fine powder. *Challenge Journal of Concrete Research Letters*, 11(1), 1–10.

Barros JAO, Figueiras JA (1999). Flexural behavior of steel fiber reinforced concrete testing and modeling. *Journal of Materials in Civil Engineering ASCE*, 11(4), 331–339.

Bazant Z, Pfeiffer P (1987). Determination of fracture energy from size effect and brittleness number. *ACI Material Journal*, 84, 463–480.

Biswajit J, Mohanty B (2015). Study on the mechanical properties and fracture behavior of chopped steel fiber reinforced self-compacting concrete. *International Journal of Engineering Research and Technology IJERT*, 4, 164–170.

Douglas R (2004). Properties of Self-Consolidating Concrete Containing Type Fly Ash with a Verification of the Minimum Paste Volume Method. *MSc. thesis*, Northwestern University, USA.

Elices M, Planas J (1996). Fracture mechanics parameters of concrete an overview. *Advanced Cement Based Materials*, 4, 116–127.

Ghazy MF, Abd Elaty MA, Dabaon O (2015). Rheological and mechanical characterization of fiber-reinforced self-compacting concrete. *1st International Conference on Advanced Structure and Geotechnical Engineering*, Hurghada, Egypt.

Groth P, Nemegeer D (1999). The use of steel fibers in self-compacting concrete. *Proceedings of the 1st International RILEM Symposium on Self-Compacting Concrete*, Sweden, 497–507.

Hoang AL, Fehling E (2017). Influence of steel fiber content and aspect ratio on the uniaxial tensile and compressive behavior of ultra high performance concrete. *Construction and Building Materials*, 153, 790–806.

Hordijk DA (1991). Local Approach to Fatigue of Concrete. *PhD Thesis*, Delft University of Technology, Netherlands.

Khayat K, Roussel Y (1999). Testing and performance of fiber-reinforced self-consolidating concrete. *Proceedings of the 1st International RILEM Symposium on Self-Compacting Concrete*, Sweden, 509–521.

Kytinou VK, Chalioris CE, Karayannis CG (2020). Analysis of residual flexural stiffness of steel fiber reinforced concrete beams with steel reinforcement. *Materials*, 13, 1–24.

Morelli F, Amico C, Salvatore W, Squeglia N, Stacul S (2017). Influence of tension stiffening on the flexural stiffness of reinforced concrete circular sections. *Materials*, 10, 669.

Okamura H, Ozawa K (1995). Mix design for self-compacting concrete. *Concrete Library of JSCE*, 25, 107–120.

Persson B (2001). A comparison between mechanical properties of self-compacting concrete and the corresponding properties of normal concrete. *Cement and Concrete Research*, 31, 193–198.

Sabir B, Wild S, Asili M (1997). On the tortuosity of the fracture surface in concrete. *Cement and Concrete Research*, 27, 785–795.

Smarzewski P, Barnat-Hunek D (2015). Fracture properties of plain and steel polypropylene fibers, *Materials and Technologies*, 49, 563–571.

Wittmann FH (2002). Crack formation and fracture energy of normal and high strength concrete. *Sadhana*, 27, 413–423.